[Trupti Kathrotia, Patrick Oßwald, Julia Zinsmeister, Torsten Methling, Markus Köhler, Combustion Kinetics of Alternative Jet Fuels, Part-III: Fuel Modeling and Surrogate Strategy, 302 (2021) 120737]

The original publication is available at www.elsevier.com

https://doi.org/10.1016/j.fuel.2021.120737

Combustion Kinetics of Alternative Jet Fuels, Part-III: Fuel Modeling and Surrogate Strategy

Authors: Trupti Kathrotia*, Patrick Oßwald, Julia Zinsmeister, Torsten Methling, Markus Köhler

Institute of Combustion Technology, German Aerospace Center (DLR), 70569 Stuttgart, Germany

*Corresponding Author: Trupti Kathrotia

German Aerospace Center, Pfaffenwaldring 38-40, 70569 Stuttgart, Germany

phone: +49-711-6862-558; email: trupti.kathrotia@dlr.de

Abstract

In Part III of our study on alternative aviation fuels, we present a comprehensive database of modeled speciation data consisting of seven hydrocarbons of varying molecular structure and 26 alternative and conventional aviation fuels. The speciation data is obtained from the DLR atmospheric high temperature flow reactor with a coupled molecular beam mass spectrometry (MBMS) detection system (Part-I). The chemical reactivity of these real liquid fuels is investigated both experimentally and numerically. For modeling, detailed fuel surrogates (up to 14 components) are employed for characterizing the fuels. The surrogate formulation strategy is defined based on the fuels' compositional analysis.

This work employs high temperature reaction kinetic mechanism for the combustion of wide variety of hydrocarbons of varying molecular classes from n-, iso-, cy-paraffins, to five-ring aromatics presented in Part-II. The reaction mechanism is applied to model 26 aviation fuels using 21 different validated fuel surrogate components to predict the fuel intermediates and soot precursors measured in the reactor.

This work aims to identify the effect of fuel surrogate components on the intermediates' formation and its influence on the emissions. Through compilation of many fuels with composition of wide range of chemical classes, we provide a systematic evaluation of how the fuel composition can be used to extract information of specific fuel intermediates and emissions formed.

Keywords: Aviation fuels, fuel surrogate, modeling, flow reactor, hydrogen deficiency

1. Introduction

The intrinsic details of combustion intermediates and their possible effect on emissions formed during the combustion of a fuel in aero engines are complex and challenging. For such investigations experimental approaches are scarce and limited in terms of technical conditions or interacting processes. Model studies are destined to overcome this boundary in the long run. For example, the computational fluid dynamic (CFD) studies can provide the complex interaction of the effects of turbulence and

chemistry. In order to include the chemical effect, one requires (1) a fuel surrogate – that simplifies the real fuel formulation and (2) reaction kinetic model – that describes combustion chemistry with a high degree of confidence.

Modeling a real fuel is extremely challenging, if one considers the multitude of chemical compounds of varying carbon numbers and molecular classes present in them. While detailed fuel design strategies benefit from a detailed chemical approach for optimization purposes [1, 2], it is still ongoing discussion if this level of detail is even necessary for covering relevant effects in combustion and predicting, e.g. pollutants. A typical approach in chemical modeling is therefore the definition of a model (surrogate) fuel [3], which considers certain representative fuel components by considering physical or chemical boundary conditions of a real fuel. In order to include combustion chemistry, one requires a reaction kinetic model that includes various hydrocarbon components of the fuel surrogate. These models are applied to explain the details of combustion chemistry and at the same time need to be compact, if required for larger dimensional model studies. Various surrogate fuels and their methodology are defined in literature since the pioneering work from Schulz et al. [4]. Prior works have shown combustion properties targets such as H/C ratio, derived cetane number, average molecular weight, sooting indexes can be used as boundary conditions to define the model surrogate that can replicate the fuels' physical and chemical behavior. Thus, various fuel surrogates of varying degree of details have been investigated in literature [3, 5-18].

Taking a closer look at the kinetic modeling side, a variety of hydrocarbons is present in real fuels. There is only a limited number of reaction mechanisms present in literature [20-23], which can resolve the differences of real fuels and additionally predict pollutants. Additional sub-mechanisms are required to predict aromatics and soot precursor species, adding to the complexity. Since these aviation fuels are comprised of multicomponent hydrocarbon mixtures, where the amount and type of hydrocarbons (molecular class) differ considerably, it is important to understand how this variation will affect (1) physical and chemical properties – for performance and safety related issues and (2) combustion characteristics including pollutant formation – for performance and environmental related issues.

Aviation fuels are strictly regulated, with severe constraints to ensure safety and compatibility. Today's alternative fuels not only focus on the safety issue, but also on the environmental aspect. The presence of aromatics is known to promote the soot emissions however a minimum aromatics content of 8.0 vol% is required for jet fuels containing synthetic components according to ASTM standard D7566-20b [24]. The aromatics in fuel are essential for swelling of certain elastomers to ensure safety of sealing properties of fuel systems [25], seals for alternative fuels are being investigated [25-27]. In absence of any technological modification with respect to aromatics-free sealing systems, a better understanding on influence of fuel bound aromatics is required for existing and more importantly for the design of new synthetic fuels. One can design a fuel containing required 8% aromatics with molecules that possesses less sooting tendency thereby fulfilling both the criteria of safety and environmental aspects. Studies

have shown that in synthetic paraffinic hydrocarbon fuels, greatest volume swell is imparted by small aromatic molecules with significant hydrogen-bonding or polar character [26, 27]. In this sense, understanding the impact of fuel components on the sooting tendency of a fuel is important. Recently, we presented a systematic evaluation of intermediates and soot precursors formations in n-paraffins [29]. Similar evaluations for other chemical classes are missing in literature. They can be important as they form the basis for understanding complex fuel mixtures. In this study, we extend this information to other molecular classes and their importance in multi-component fuel mixtures. The single fuel components n-decane, farnesane, propyl-cyclohexane, n-propylbenzene, decalin, tetralin, and methylnaphthalene, to cover the n-, iso-paraffins, mono- and di-cyclo-paraffins as well as mono- and di-aromatics and fused cyclo-aromatics ring structure, are studied at constant carbon flow condition. By doing so, we cover a wide range of molecular classes. The information obtained from single components will be useful for understanding of complex fuel mixtures. Many chemical kinetic studies are available in literature investigating the oxidation of different hydrocarbons. Compared to n-, iso- and cyclo-paraffins, information on the aromatics and complex cyclo-aromatics is limited. None of the studies provide information on all the hydrocarbon types at similar combustion conditions for direct comparison. This is particularly important as conventional transportation fuels contain many of the less studied hydrocarbons (e.g. tetralin, decalin in gasoline, diesel, and jet fuels). As discussed in Part II of this paper series [19] only limited reaction models in literature support predictions of various hydrocarbons including soot precursor chemistry [20-23]. Following these mechanisms for modeling real fuels, we present a single reaction mechanism containing 70 different hydrocarbon components for the description of different fuels used in aviation (jet fuel) or in road transportation (gasoline, diesel) including soot precursor chemistry. A detailed description and validation of these compounds that are implemented in the present work are available in Part II of this paper series [19] and this part focuses on covering conventional and alternative real aviation fuels.

A wide range of studies are available in literature investigating mainly single fuels. Discussion on inferences from multiple fuels studied at similar conditions is rather limited. A systematic evaluation of fuels with respect to their composition is still limited and mostly focused on global combustion characteristics. From these studies, there are numbers of questions that are open (1) how does the fuel's molecular structure influence intermediates (2) what are the factors affecting soot precursors formation. Gas-to-liquid (GtL) and coal-to-liquid (CtL) alternative jet fuels and their surrogates were investigated in jet-stirred reactor by Dagaut et al. [30], here no particular attention to the influence of surrogates' molecular structure on combustion products is highlighted. A global reactivity of variety of conventional and alternative fuels investigated in [31] showed no major variation in the extinction limit of diffusion flames of all fuels. Ignition delay times of a variety of fuels are also investigated in various recent studies [10, 31-36]. In general, these limited number of studies show at high temperatures (>1000 K) the global reactivity is similar for fuels measured as either ignition delay times, flame speeds or fuel-oxidizer conversion [10, 31, 33, 35, 36]. Proceeding to the effect of fuels burning, equally important aspect in

fuel usage is the emissions. The studies on influence of cyclic components present in fuels on soot (precursors) are scarce [37, 38]. Saggese et al. [38] showed that the soot in nucleation-controlled flame is more influenced by presence of high-boiling distillates, which are essentially multi-ring aromatics, than in surface growth-controlled flames. Implications of quality of aromatics on soot precursor formation using two fuels is studied in [37], who showed that the relation between H-content of fuel and soot formation tendency is not universally applicable and rather the quality of aromatics can be more effective way in soot reduction. This is similar to our earlier work [39] where based on the unsaturation and cyclic content of fuel, we showed that the trend in soot emissions can be related.

None of these studies investigate soot precursors in series of aviation fuels at similar conditions. In this context, focusing on the combustion characteristics, we studied 26 different reference and alternative aviation fuels for a systematic approach and present their differences in intermediates and product formation. The chemical reactivity of the fuels is investigated in a high temperature DLR flow reactor, where more than 25 species concentrations for each fuel are obtained and investigated both experimentally and numerically, details in [28]. Two fuel stoichiometries are investigated for this purpose. A detailed fuel surrogate is employed for modeling the fuels. We compared the main products, intermediates and the soot precursor formed during the combustion of these fuels and discussed how the fuel composition influences the intermediate formation and their tendency to form different soot precursors. This work provides an important experimental database on soot precursors formed during the combustion of large number of fuels at constant combustion condition and implications derived from model-experiment comparison.

The purpose of this study is two-fold: validate and present a detailed mechanism to cover the compositional influence on the reaction chemistry of conventional and alternative jet fuels (and beyond); special emphasis is given to the soot precursor chemistry and its relation to the composition of the complex real liquid fuels. This is achieved by (1) Investigating the maximum hydrocarbon type (individually) at similar conditions and (2) investigating the influence of individual hydrocarbon type in a mixture, particularly in aviation fuels.

The next sections include the fuels, the fuel surrogate – strategy, selection and properties. The chemical reactivity of fuels is discussed in detail considering first C_1-C_4 intermediates, then small and large aromatics. The large model/experiment dataset of 26 fuels and 7 components allows a systematic evaluation on influence of certain molecular class(es) on the formation of specific fuel intermediates and soot precursors.

2. Fuels investigated

Although many reports on different fuels are available in literature, most of them are investigated at different conditions, and therefore difficult for general interpretations. In this aspect, our study of 26

different alternative and conventional fuels [28] of wide variation in composition and 7 different fuel components [19] individually all at same condition provides a direct comparison to understand the global and individual combustion and emission behavior of the complex aviation fuels.

In this work the aviation (alternative and reference) fuels investigated, based on their production processes, are categorized into five different fuels (1) Fossil based, (2) Fischer-Tropsch (FT) fuels, (3) Alcohol-to-jet (ATJ) fuels, (4) Synthetic Iso-Paraffins (SIP) fuels obtained from hydro-processed sugar fermentation, and (5) Hydroprocessed Esters and Fatty Acids (HEFA) fuels. More details on the fuels can be found in Part-I of this paper series [28].

The investigated fuels are summarized in Table 1 with information on production process, their hydrogen content w_H, and index of hydrogen deficiency (IHD) [39] used later in the results to characterize the emission behavior of fuels and short name for discussion.

Table 1: Summary of fuels studied in this work [28].

	Fuel	Group	Short name	w_H (%m/m)	IHD
1	FT-Light	FT	FT-Light	15.12	0.266
2	SIP (farnesane)	Alc./Sug.	Farnesane	15.09	0.000
3	JETSCREEN JS-B1	Alc./Sug.	JS-B1	15.31	0.001
4	ATJ-SKA	Alc./Sug.	ATJ-SKA	14.61	0.780
5	airegEM ReadiJet® (JS-B3)	HEFA	JS-B3	13.60	1.834
6	ACCESS HEFA Blend (50:50)	HEFA	Acc-HEFA50	14.42	0.948
7	ECLIF FSJF	FT	E1-FSJF	14.17	1.113
8	ECLIF Ref 1	Fossil	E1-Ref1	13.67	1.460
9	ECLIF Ref 2	Fossil	E1-Ref2	13.73	1.451
10	ECLIF SSJF 1	FT	E1-SSJF1	14.36	0.851
11	ECLIF SSJF 2	FT	E1-SSJF2	14.53	0.763
12	ECLIF SSJF 3	FT	E1-SSJF3	14.01	1.277
13	ECLIF2/ND-MAX Ref 3	Fossil	E2-Ref3	13.65	1.624
14	ECLIF2/ND-MAX Ref 4	Fossil	E2-Ref4	14.08	1.251
15	ECLIF2/ND-MAX SAJF 1	HEFA	E2-SAJF1	14.40	0.903
16	ECLIF2/ND-MAX SAJF 2	HEFA	E2-SAJF2	14.51	0.891
17	ECLIF2/ND-MAX SAJF 3	HEFA	E2-SAJF3	14.04	1.255
18	JETSCREEN JS-A1	Fossil	JS-A1	14.02	1.341
19	JETSCREEN JS-A1.3	Fossil	JS-A1.3	14.43	0.886
20	JETSCREEN JS-C1	-	JS-C1	12.66	2.859
21	SASOL IPK	FT	S-IPK	15.34	0.048
22	SASOL IPK-A	FT	S-IPK-A	14.31	1.022
23	SASOL Heavy Naphtha #1	FT	S-HN1	14.79	0.616
24	SASOL Heavy Naphtha #2	FT	S-HN2	12.57	2.367
25	SASOL Light Distillate #1	FT	S-LD1	14.01	1.240
26	SASOL Light Distillate #2	FT	S-LD2	12.87	2.379

3. Fuels - Experiments and Reaction model

The measurements presented in this work employ a high temperature flow reactor to obtain speciation data of various fuels and single fuel components. The details of the experimental conditions [28] and

experimental setup are presented elsewhere [29, 40-43]. The experiments are performed in the temperature range of 700 to 1250 K, at ambient condition and for fuel stoichiometries of Φ = 0.8 and 1.2. These experiments are performed at the same carbon flow enabling a direct comparison to investigate the influence of molecular structure on the soot precursors' formation. A brief description of the input conditions modeled in this work can be found in the supplemental material and in more detail in Part I of this series [28].

In present work, 21 different hydrocarbons components are used in the modeling of fuel surrogates. Here the individual fuel component validation [19] supplies the basis for the model which can be used for the interpretation of complex fuel mixture. The DLR reaction mechanism presented in this work is a single reaction mechanism that includes reaction chemistry for the description of n-paraffins C_1-C_4, C_6-C_7, C_9-C_{10}, C_{12}, and C_{16}, iso-paraffins such as iso-octane (2,2,4-trimethyl-pentane), one methyl branched $iC_{11}H_{24}$ (2-methyl decane), as well as $iC_{10}H_{22}$ (2,7-dimethyl-octane), and farnesane $iC_{15}H_{32}$ (2,6,10-trimethyl-dodecane), cyclo-paraffins such as cyclohexane, n-propylcyclohexane, decalin, cyclo-aromatics such as indane, indene, tetralin, and number of aromatics such as benzene, toluene, propylbenzene, styrene, naphthalene, methylnaphthalene and biphenyl. In addition to the common molecular families present in alternative and conventional jet fuels, some higher polycyclic aromatic hydrocarbons PAHs (e.g. phenanthrene, pyrene, polyynes up to C_{10}) up to C_{20} are implemented as fuel molecules and enable adjustment of the sooting propensity of a given fuel when desired. The reaction mechanism is validated over large set of experimental data; a complete description of the mechanism is available in [19]. The reaction mechanism includes 238 species, 1814 reactions. The chemistry related to fuels' combustion intermediates and soot precursors chemistry is discussed in Sec. 6. A small change related to reaction rate of $CH_2O+H=HCO+H_2$ is considered in this work in order to improve H_2 predictions in the flow reactor. This change however presents no visible change in any of the resulting soot precursors predictions except small increase in CH_2O. All the fuels are calculated with the same mechanism. To have one mechanism provides the advantage, where the uncertainty related to model can be subdued when comparing species predictions with respect to their fuel composition.

4. Modeling - Fuel Surrogate Strategy

Initially (in the last decade) the focus of the fuel model surrogate has been to replicate the global combustion behavior of the jet fuels. The surrogate fuels are typically a mixture of one to four components that can reasonably emulate the physical and chemical properties of real fuel [3, 5-18, 37, 44]. More information is available in the comprehensive review papers of Pitz and Mueller [45] and Battin-Leclerc et al. [46]. Typically, these investigations are focused on a conventional or "average" Jet A1 or JP8, respectively. Compositional deviation of individual jet fuels on various combustion properties is often not focused until in the recent years. With the focus shifted to the pollutant emissions reduction and use of new fuels from a variety of alternative sources and compositions, it has become

more important to increase the detailing of the fuel surrogate used for the understanding of the combustion and emission performance within the combustor. One of the key elements in understanding the underlying systematics is the composition of the fuel.

4.1 Fuel Composition

Based on the two-dimensional gas chromatography (GCxGC) analysis, the fuels' composition of present work can be categorized by six major molecular classes namely, n-, iso-, and cyclo-paraffins containing one or two rings, as well as mono- and di-aromatics and cyclo-aromatics. The compositions of the investigated fuels are shown in the Fig. 1. For convenience of later discussion, the fuels are divided into four categories: (A) n-/iso-paraffins based fuels, (B) fuels containing aromatics ≤10%, (C) fuels containing aromatics 13-20% and last category (D) fuels containing total cyclic content of >65%. This categorization was made for the later discussion on influences and effects between fuel composition, soot precursors and intermediate pools.

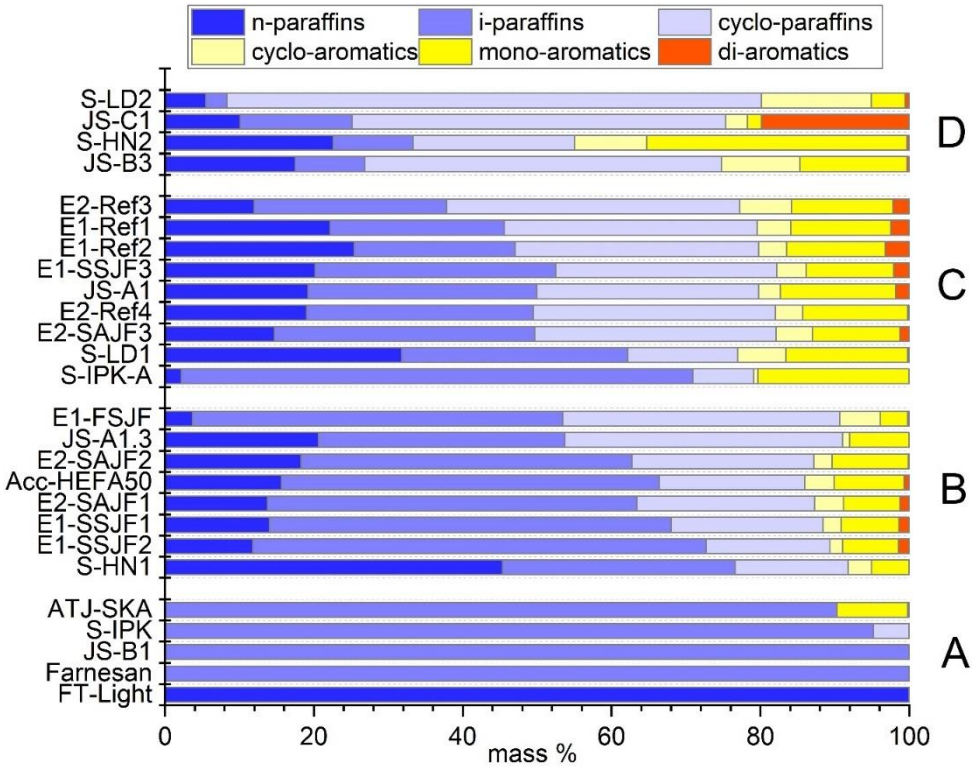

Fig. 1: Composition of fuels studied in this work distinguished by structural classes of hydrocarbons present [28].

4.2 Fuel surrogate approach

A numerical investigation of a liquid fuel is complicated by the fact that real fuels contain hundreds of chemical compounds, each of these are impossible to employ even in a simplest (low dimensional) numerical investigation. For this reason, a fuel surrogate, simplified definition of fuel involving limited set of fuel component species is beneficial to emulate the real fuel. The selection of surrogate

components and subsequently their compositions are then estimated based on the boundary conditions defined such as chemical properties and/or physical properties of real fuel.

Several strategies for the selection of fuel surrogates are employed in the literature, often based on real fuel compositions [47-49], and/or relevant physical properties such as (e.g., viscosity, surface tension, density, distillation curve, heat of combustion, etc.) [50, 51], or combustion properties targets (e.g. combustion related properties such as ignition, heat release, extinction limit, lean blowout limit, sooting tendencies of fuel etc.) [9, 16, 52]. Dryer et al. [9, 10, 16] demonstrated that by matching four combustion properties targets (derived cetane number, H/C, threshold soot index, average molecular weight) of a specific fuel is sufficient to display the pre-vaporized global combustion kinetic behavior. Later similar results were obtained using distillation cuts of molecular classes of hydrocarbons [10]. Earlier in 2001 Edwards and Maurice [6] pointed out that in order to consider the gas phase kinetic behavior of a real fuel, it is important to consider the fuel by their molecular class. Huber et al. [44] showed that the inclusion of multiple alkanes specifically low and high molecular weight n-paraffins can be useful to achieve the desired initial boiling behavior and tail of the distillation curve whereas iso-paraffins can help to accurately predict the thermal conductivity of the target fuel. The general combustion behavior could be achieved by selecting few target molecular classes, the final selection should to be based on the end focus of the study. In general, combustion studies focused on their chemical characterization employ gas phase, where the aim is the predictive character of i.e. intermediates, pollutants estimation. The studies related to intrinsic details of physical properties of a fuel e.g. spray characteristics can be modeled with other methods that do not rely on single molecules.

In this work, detailed fuel surrogates (up to 14 components) are considered for characterizing the fuels listed in Fig. 1. The surrogates' definition is based on the compositional analysis of the fuel obtained through GCxGC analysis. It is known from previous studies that the n- and iso-paraffins possess similar global combustion characteristics and the (pre-vaporized) combustion characteristics are nearly independent of the carbon number [53-56]. Therefore, for n-paraffins, mainly one representative hydrocarbon is selected. For fuels containing dominantly iso-paraffins, four different paraffins (differs in degree of branching) are used for the surrogate definition. This was restricted to one iso-paraffin for fuels containing a significant amount of cyclic components in order to reduce the complexity of the surrogate. The fuels containing cyclic compounds even in smaller amounts compared to straight chain and branched paraffins can also have a significant influence on the soot emissions [39]. Therefore, multiple cyclo-paraffins and aromatic species are selected for the fuel surrogate. Multiple aromatic species amounting to even less than 1% are considered in the surrogate formulation, specifically di-aromatics are intensively considered as studies have found their significant influence on PAH formation when present even in small amount [37].

The composition of a surrogate selected from the composition obtained from GCxGC is depicted in schematic (Fig. 2). Since the present study focuses on gas phase kinetics, we have selected molecular

classes and carbon numbers based on the GCxGC analysis of the fuel. As seen in Fig. 2, the composition (mass fraction) obtained from the analysis is available as a function of the carbon number and molecular class. The selection of fuel surrogate components within a particular molecular class (and carbon number) will also depend on the existence of the species in the reaction mechanism. Initially for every molecular class, 1 to 3 species of varying carbon number with maximum share/proportion is selected. The rest of the portion (not selected C-number) is summed to selected ones according to the nearest carbon number. At the same time total share is kept fixed within given molecular class. With an aim to study soot precursors, as stated earlier, the number of n- and iso-paraffins are restricted to only one species whereas multiple cyclo-paraffins and aromatics are selected depending on the availability in the reaction mechanism and their amount present. Aromatics, specially di- and poly-aromatics, were carefully considered and when available, even <1% were considered separately.

Multiple cyclo-paraffins and aromatics are selected to represent the typical molecular class and carbon number, where the composition maximum occurs. Biphenyl is considered as representative of di-aromatics except in three Sasol fuels where it has been chosen as representative for C_{12} naphthalenes. The selection of e.g. acenaphthylene ($C_{12}H_8$) has been chosen as representative for C_{12} di-aromatics, even if not constituent of the fuels it is chosen purely based on the availability of a particular molecule in the reaction mechanism (Fig. 2).

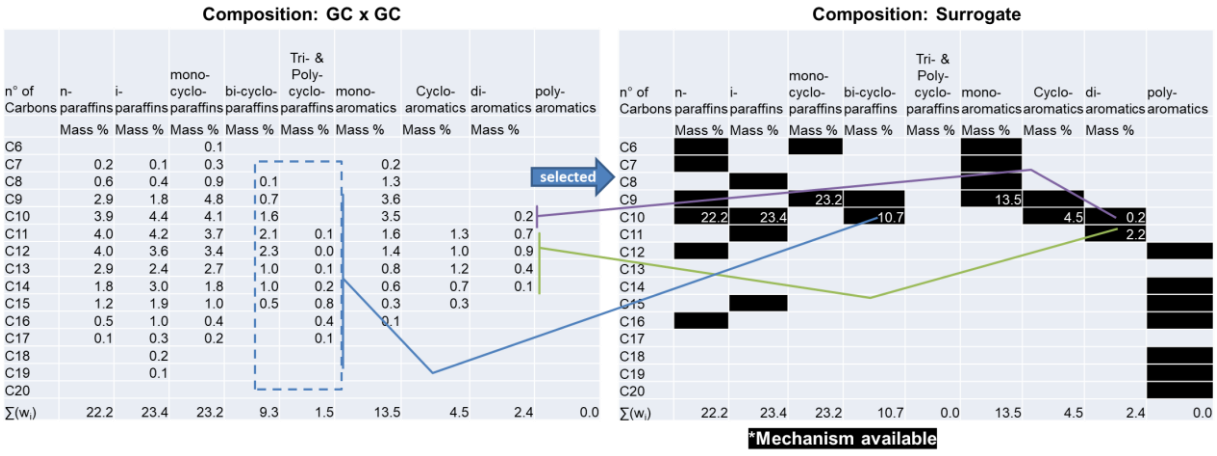

Fig. 2: Example of surrogate determination using composition analysis of fuels (E1-Ref1) translated to fuel surrogate.

To conclude, our definition of the surrogate fuel contains a maximum of 14-components for the detailed description of the fuel composition. For the fuel surrogate, 21 different model components are used for the fuels' surrogate definition. The mass fraction of a selected component (translated from GCxGC) is converted to corresponding mole fractions for the surrogate fuel. The mass composition and the selected hydrocarbon components of the 26 fuel surrogates are summarized in Table 2. The details on available fuel molecules in the reaction model are available in Part II [19].

Table 2: Composition of studied fuel surrogates, data in mass%.

Surrogate Component* (%m/m) →	n-C_7	n-C_9	n-C_{10}	n-C_{12}	i-C_8	i-C_{10}	i-C_{11}	i-C_{15}	C_9H_{18}	$C_{10}H_{18}$	C_7H_8	C_8H_{10}	C_9H_{12}	C_9H_{10}	C_9H_8	$C_{10}H_{12}$	$C_{10}H_8$	$C_{11}H_{10}$	$C_{12}H_{10}$	$C_{12}H_8$	$C_{14}H_{10}$
FT-Light	10.7	27.1		62.2																	
Farnesane								100													
JS-B1					70.0		15.8	12.3													
ATJ-SKA					29.8		29.8	29.8					9.5								
JS-B3			17.5			9.4			30.6	17.3			14.4	0.6	1.4	8.5	0.02	0.2	0.035		
Acc-HEFA50				15.5			50.3		15.2	4.2			9.4	0.04		3.9	0.05	0.3	0.1	0.1	0.020
E1_FSJF			3.7				49.7		13.1	24.1			3.7			5.4	0.02	0.2			
E1_Ref1			22.2			23.4			23.2	10.7			13.5			4.5	0.2	2.2			
E1_Ref2			25.4				21.7		22.6	10.1			13.3			3.7	0.3	2.9			
E1_SSJF1			14.0				54.0		14.5	5.9			7.8			2.4	0.1	1.3			
E1_SSJF2			11.8				61.0		11.8	4.8			7.5			1.7	0.1	1.3			
E1_SSJF3			20.2				32.3		20.5	9.1			11.7			4.0	0.2	1.9			
E2_Ref3			12.0				25.8		23.6	15.8			13.6		1.3	5.6	0.2	1.7	0.2	0.012	
E2_Ref4			19.0			30.4			24.0	8.6			14.2		0.6	3.1	0.04	0.1	0.023		
E2_SAJF1			13.7			14.7	35.0		15.0	8.9			7.6		0.7	3.1	0.1	0.9	0.2		
E2_SAJF2			18.3			18.0	26.5		18.6	5.9			10.2		0.4	2.0	0.023	0.1	0.03		
E2_SAJF3			14.7			34.9			21.3	11.1			11.8		0.9	3.9	0.1	1.0	0.2		
JS_A1			19.2			12.8	17.9		21.8	8.0	0.1	2.2	13.1	0.1	0.6	2.3	0.2	1.5	0.1		
JS_A1.3			20.6			33.1			26.5	10.7	0.1	1.3	6.6	0.02	0.2	0.8					
JS_C1				10.1				15.0	16.4	33.8			1.9	0.1	0.4	2.5	2.0	16.1	1.7	0.1	
S-IPK-A			2.2			13.7	55.0		7.2	1.0			20.4	0.1		0.4					
S-HN1			45.4			31.2			9.5	5.7			7.8			0.4	0.005	0.004			
S-HN2			22.6			10.7			12.3	9.4	0.1	12.9	21.9	4.2		5.5	0.3	0.040	0.006		
S-LD2				5.5			1.4	1.4	17.6	54.2			4.5			14.8	0.04	0.2	0.3		0.1
S-IPK						23.7	61.2	10.4	4.8					0.003		0.013					
S-LD1				31.7			30.3		12.6	2.2			16.3			6.4	0.030	0.1	0.1		

*Details of surrogate components in table: n-C_7 (n-heptane), n-C_9 (n-nonane), n-C_{10} (n-decane), n-C_{12} (n-dodecane), i-C_8 (iso-octane), i-C_{10} (2,7 dimethyl-octane), i-C_{11} (2-methyl decane), i-C_{15} (farnesane), C_9H_{18} (n-propylcyclohexane), $C_{10}H_{18}$ (decalin), C_7H_8 (toluene), C_8H_{10} (ethylbenzene), C_9H_{12} (propylbenzene), C_9H_{10} (indane), C_9H_8 (indene), $C_{10}H_{12}$ (tetralin), $C_{10}H_8$ (naphthalene), $C_{11}H_{10}$ (1-methylnaphthalene), $C_{12}H_{10}$ (biphenyl), $C_{12}H_8$ (acenaphthylene), $C_{14}H_{10}$ (phenanthrene).

4.3 Chemical and Physical Properties

To assess the credibility of the selected fuel surrogates, their chemical and physical properties are compared to their corresponding real fuels. For fuel surrogates, the property of the mixture is obtained from the neat components using linear mixing rules. The properties data of neat components are extracted from DIPPR database [57]. Since the prediction of cetane number based on chemical kinetic calculation is a complex issue, we have not targeted this specific value yet. The H/C ratio and the molar mass of both fuels and fuel surrogates are shown in Fig. 3. H/C values of the fuels rely on the hydrogen content measurements by nuclear magnetic resonance spectroscopy NMR (ASTM D7171), while the molar mass was either directly obtained from the composition (measured by GCxGC) or estimated based on the T50 boiling point and density following the correlation by Lee and Kesler [58].

The deviations between the H/C ratios of the fuel and its surrogate are less than 2%, whereas the molar mass of most of the fuel surrogates can be achieved within 10%. Deviations up to 15% in molar mass are seen for three fuels S-LD2, JS-B3, and JS-C1. The main reason for deviations in JS-B3 and JS-C1 is the presence of large di-aromatics C_{10}-C_{16} in the real fuel which are available in model as C_{10} and C_{11}. Similarly, S-LD2 contains about 13% cyclo-alkylbenzenes (C>10) which is taken as C_{10} in the model.

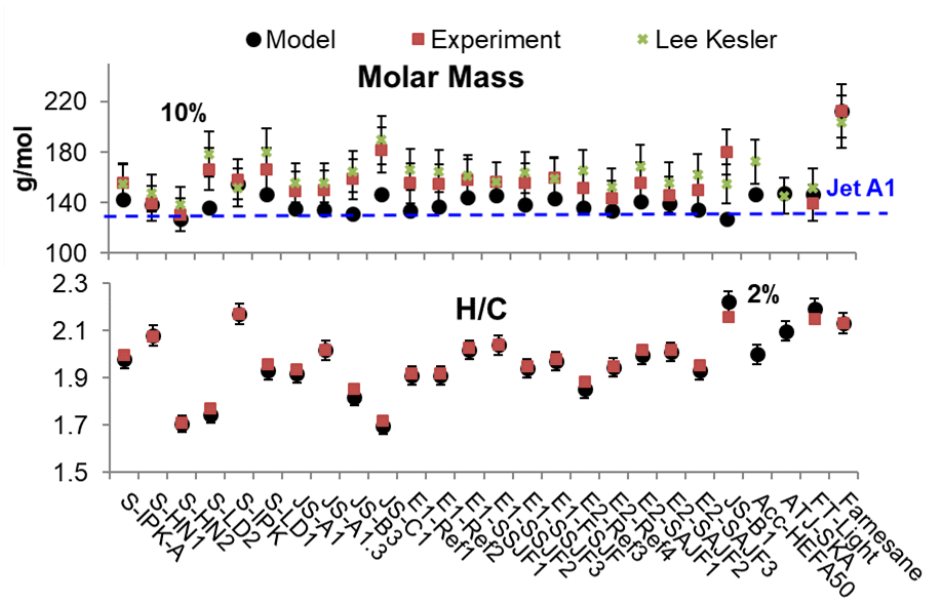

Fig. 3: Comparison of molar mass and H/C ratio of fuel (experiment) and fuel surrogates (model).

The physical properties of the fuel surrogates are compared to the standard specifications of Jet A1 and synthetic kerosenes. Fig. 4 shows two physical properties relevant for jet fuels viscosity, density, as well as chemical property such as specific energy. The specific energy of some of the fuels available is compared to respective standard ASTM methods. The specific energy of fuel surrogates is within 5% of measurements. The viscosity of the fuel surrogates at -20°C are in good agreement with the uncertainty of measured data that is usually less than 5%, except FSJF which is 15% off the measurement. Similarly, the density data for all fuel surrogates agree within 5% of the fuels' measurements.

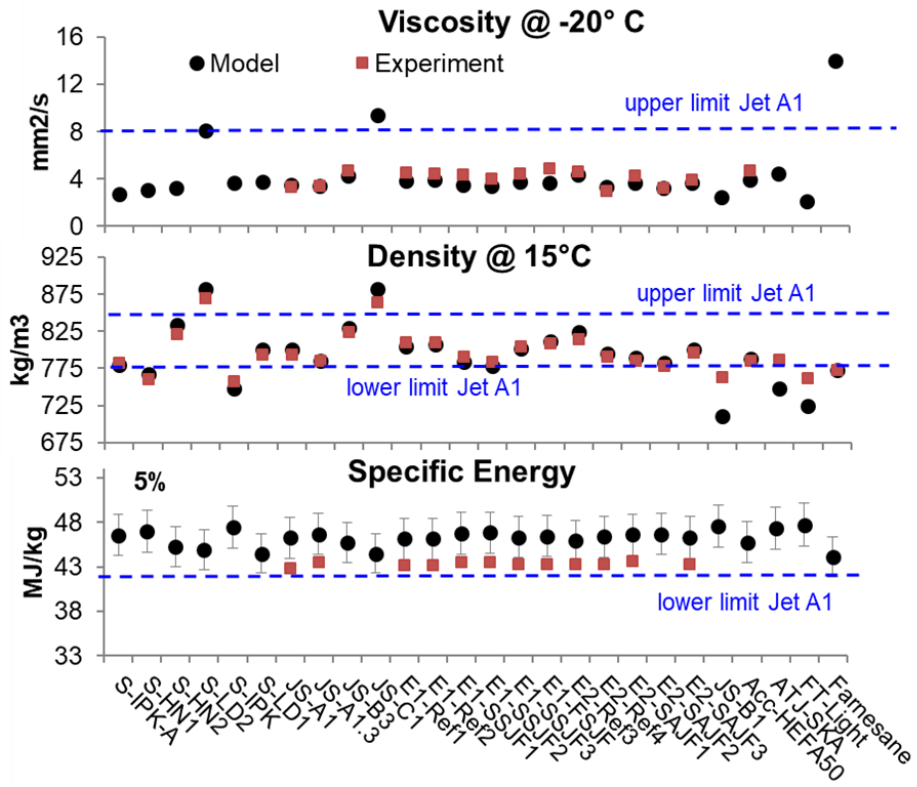

Fig. 4: Comparison of measured physical and chemical properties of fuel with calculated fuel surrogates.

Another important parameter is distillation curves. A comparison of the initial boiling point (IBP), temperatures at 10%, 50%, and 90% v/v distilled (T10, T50, T90 respectively), and the final boiling point (FBP) of fuel with estimated data for the fuel surrogate distillates are presented in Fig. 5. The distillation curves for the fuels are measured using standard ASTM D86 method or equivalent. It is important to note that the standard ASTM D86 does not reflect the boiling point distribution in a strict thermodynamically sense as vapor-liquid equilibrium is not accurately captured and thus is limited by non-idealities that affect the measurement of the light and heavy tails. The estimation of distillation curve is based on the Soave-Redlich-Kwong (SRK) equation of state where the required data of boiling temperature, critical temperature, critical pressure and acentric factor for individual hydrocarbons present in fuel surrogate are obtained from the DIPPR database [57]. The IBP, T10 and T50 are excellently reproduced by the fuel surrogates. A maximum of 20% deviation is seen between modeled and measured T90 and FBP of data presented in Fig. 5. Thus, distillation data for fuel surrogate are in excellent agreement with the measurement, considering the non-idealities of ASTM D86 and the fact that the fuel surrogates are not specifically designed to optimize the distillation properties of fuels. The detailed distillation curves for all fuels are presented in supplemental material.

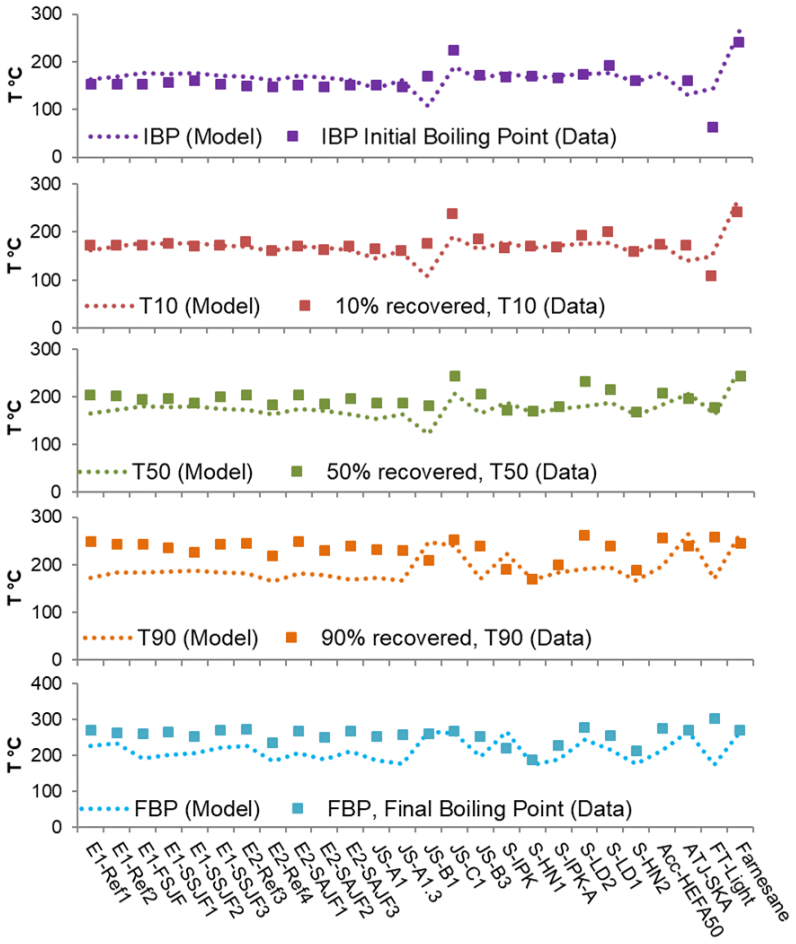

Fig. 5: Comparison of initial boiling point (IBP), T10, T50, T90 and final boiling point (FBP) of the fuels and fuel surrogate studied in this work.

In general, the fuel surrogates give a very good representation of the fuels' basic properties and can be employed reliably to represent the respective fuels.

5. Discussion – Chemical reactivity of fuels and individual fuel components

In the following we present the conversion of 7 single components covering maximum molecular structural classes present in a complex fuel mixture and are presented along with aviation fuels. The single components studied are n-decane (n-paraffin), farnesane (iso-paraffin), n-propylcyclohexane (mono-cyclo-paraffin), decalin (bi-cyclo-paraffin), n-propylbenzene (mono-aromatics), tetralin (cyclo-aromatics), and methylnaphthalene (di-aromatics) which are also present as surrogate component in model fuel.

5.1 Fuel conversion and global reactivity

Fig. 6 shows the comparison of the chemical reactivity in terms of oxygen conversion and water formation of different neat hydrocarbons as well as all real fuels measured in the flow reactor [28]. In general, except tetralin and methylnaphthalene, the conversion of all components is similar and varies

within ~50 K temperature. The temperature measurement uncertainty is about ±10 K. The conversion of tetralin is slower than all fuels whereas the conversion of methylnaphthalene is much slower compared to other components. The methylnaphthalene appears to be most stable and is consumed roughly after 1050 K, much later than all the other single component fuels are consumed. From the model analysis, this is observed due to the formation of resonantly stable intermediates naphthaldehyde from the methyl-naphthyl radical which persist in the intermediate temperatures (850-1100 K) until consumed to form naphthyl radical. Compared to the neat components, the chemical reactivity of all the fuels studied in this work is quite similar (within ΔT = 40 K) and influence of individual component, such as in methylnaphthalene is not visible, evidently due to their lower percentages in a fuel mixture (usually 1-2%) where bulk of fuel reactivity is governed by components with weaker bonds that initiates the chain reactions. Similarly, the oxygen consumption is slower in bicyclic tetralin and methylnaphthalene. Only few studies are reported in literature where comparison of variation in chemical reactivity of various fuels and components from different molecular class is presented.

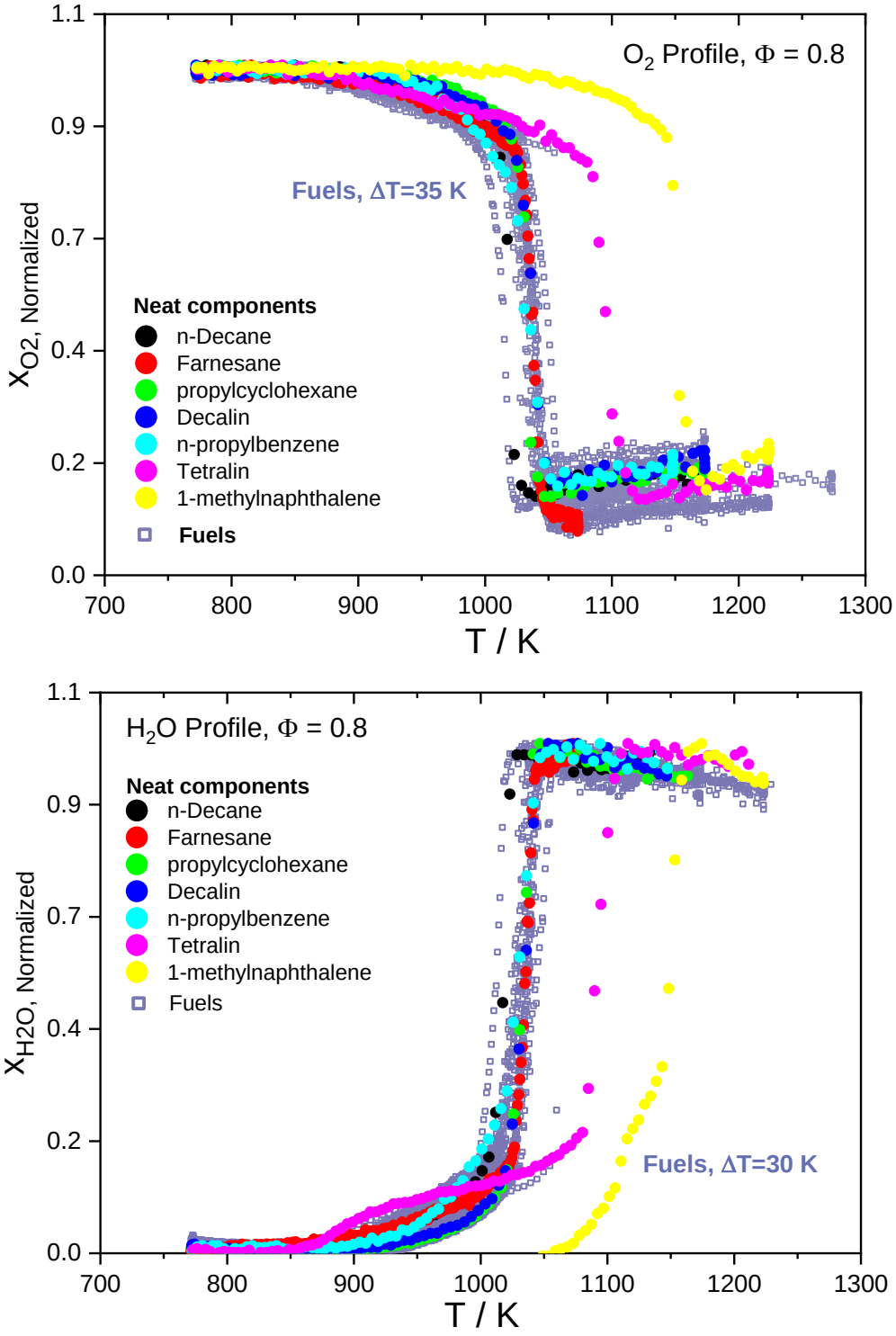

Fig. 6: Comparison of chemical reactivity of different fuel and neat components as function of oven temperature obtained in an atmospheric flow reactor. For clarity, only measurement data are shown.

Similarly, the chemical reactivity of various certified and alternative aviation fuels has also been reported representing the global characteristics such as ignition delay times and flame propagation, which are found to be comparable for various fuels. For example, Fig. 7 shows ignition delay times and flame speeds of alternative fuels such as farnesane, ReadiJet™ (JS-B3), ATJ-SPK, and ATJ-SKA are similar to Jet A1. More discussion on the influence of individual components on fuel reactivity can be

found in [19]. The comparison of ignition delay times of more than 10 conventional and alternative jet fuels investigated by Davidson and Hanson group [32] also revealed small differences in their global activation energies. Similar results were reported [33] where differences among the ignition delay measurements of fuels from diverse sources such as FT-fuels, ATJ, direct sugar to hydrocarbon (DSHC) fuels, diesel like bio-jet and conventional JP-8 were negligible (roughly within 25% of mean value which is close to the shock-tube measurement uncertainties of ~20%). This is consistent with other studies such as [35, 36] were at high temperatures (>1000 K) reactivities of conventional and alternative fuels were found to be indistinguishable. With respect to laminar flame speeds, minor scatter within the measurement uncertainties among the fuels were also reported by Won et al. [31].

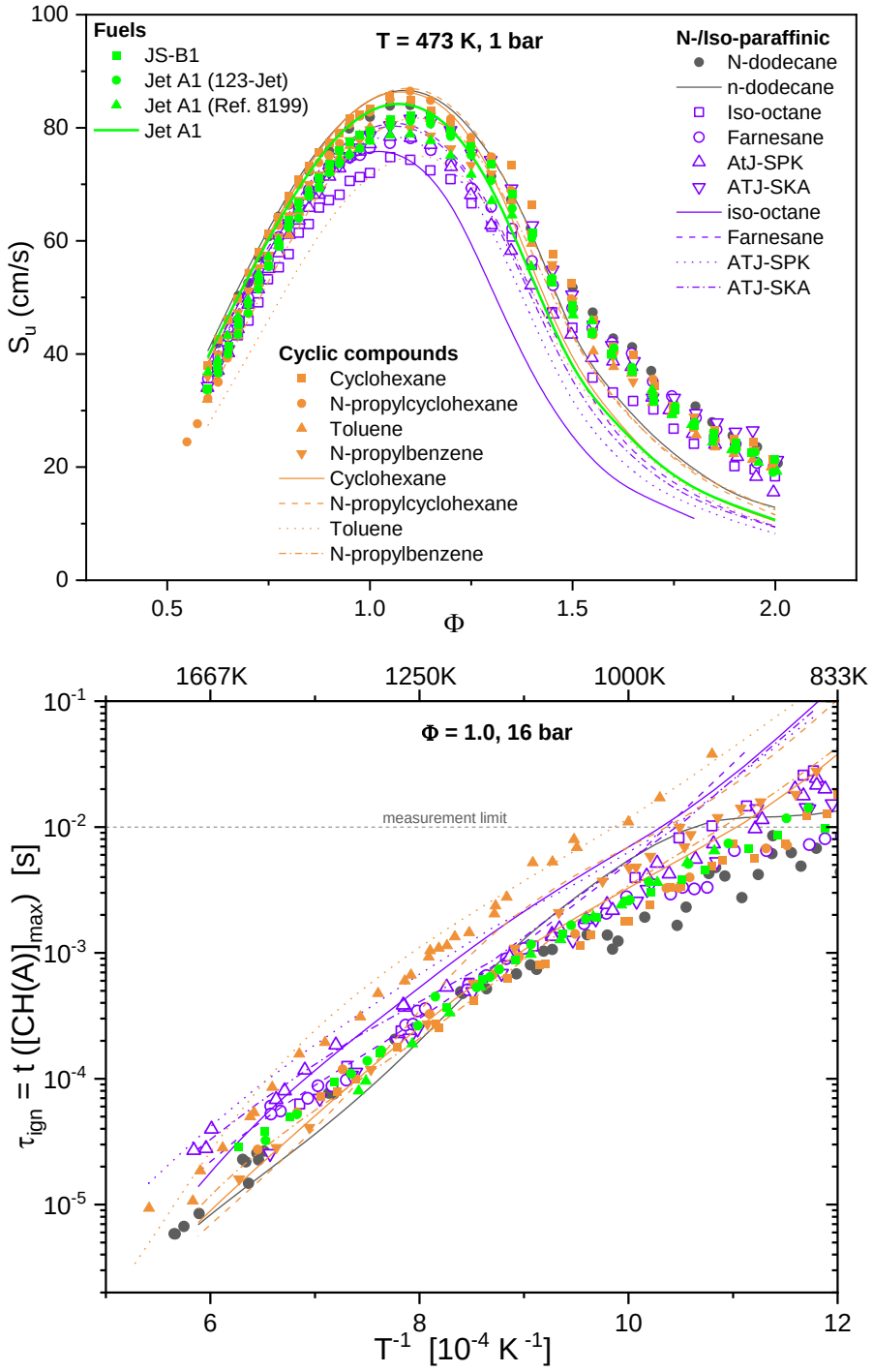

Fig. 7: Ignition delay times and flame speeds of various fuels measured in a high temperature shock-tube and laminar conical flame. Experiments: fuels [59], components: [60]. Model predictions are shown by curves.

Considering the reactivity of fuels, Dryer et al. [10] showed using Jet A and different fuel surrogates that the global reactivity of them were similar irrespective of the surrogate used. Through the measurements of about 10 alternative and JP-8 fuels in a variable pressure flow reactor by Won et al. [31] a difference in reactivity is observed at low temperatures however less variation above 1000 K, is consistent with other studies. This result can be extended to our study which shows that the reactivity of all different fuels and surrogates of 14 different component of varying amount show no general variation

in the global oxidative behavior. This is also visible from the ignition delay times obtained in a shock-tube as well as the laminar burning velocities. In addition to the fuel conversion in the flow reactor, the major products formed in all fuels are also essentially indistinguishable which shows that the net reactivity of the intermediates formed by all fuels at the conditions of our measurements is equal. Similar conclusions were also drawn by Dryer et al. [10, 31], by Hai Wang et al. [35, 61] in their fuels studied.

6. Model Predictions – Speciation

This section presents the results of modeled fuel surrogates and their intermediates and products obtained from fuels measured in the flow reactor. Since a large number of fuels is involved in this study, we present the model predictions of 5 selected fuels, categorized by dominance of each molecular class, for all reactor temperatures. For the complete data set only maximum mole fractions are compared with the measurements. For guidance, these figures are presented as bar charts containing maximum mole fractions of given species for all fuels. The plots are presented such that (1) a general model validation against the experiments including measurement uncertainties can be seen, and (2) the data are compared with the amount of various fuel components to identify trend (if any) with respect to particular molecular class(es). The generalize trend of intermediate species formed to the bulk of molecular structure is presented in this section.

6.1 Major products

For a given stoichiometry, the carbon flow is kept constant for all fuels measured as shown in the CO_2 formation in Fig. 8. The intermediates formed during combustion demonstrate the different dependences on the fuel molecules. Fig. 8 compares the measured and predicted maximum mole fractions of the oxidizer, major products CO, CO_2, H_2O, as well as H_2, and CH_2O. The measured data are plotted along with their 20% measurement related uncertainties. In general, all these species are modeled within the experimental accuracy except for modeled CO mole fractions which are consistently higher than the measurements. This could be related to model uncertainty in neat components which are however not observed in the JSR studies [19]. The maximum mole fractions of formaldehyde are also about factor of two higher in the model. The concentration of major species presents no specific dependence on the fuel composition.

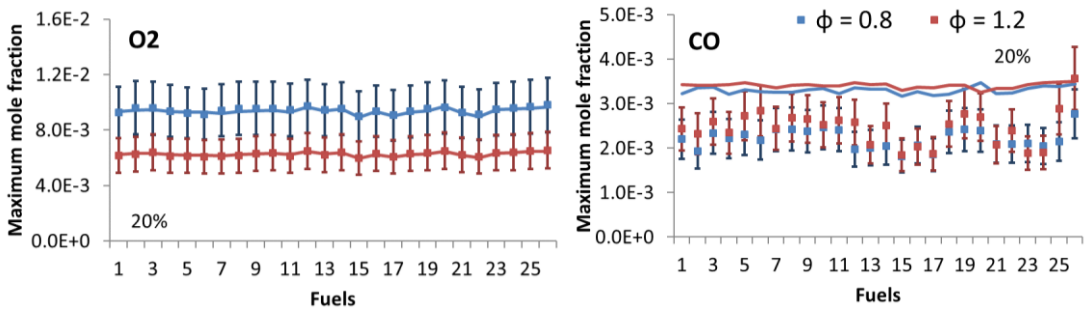

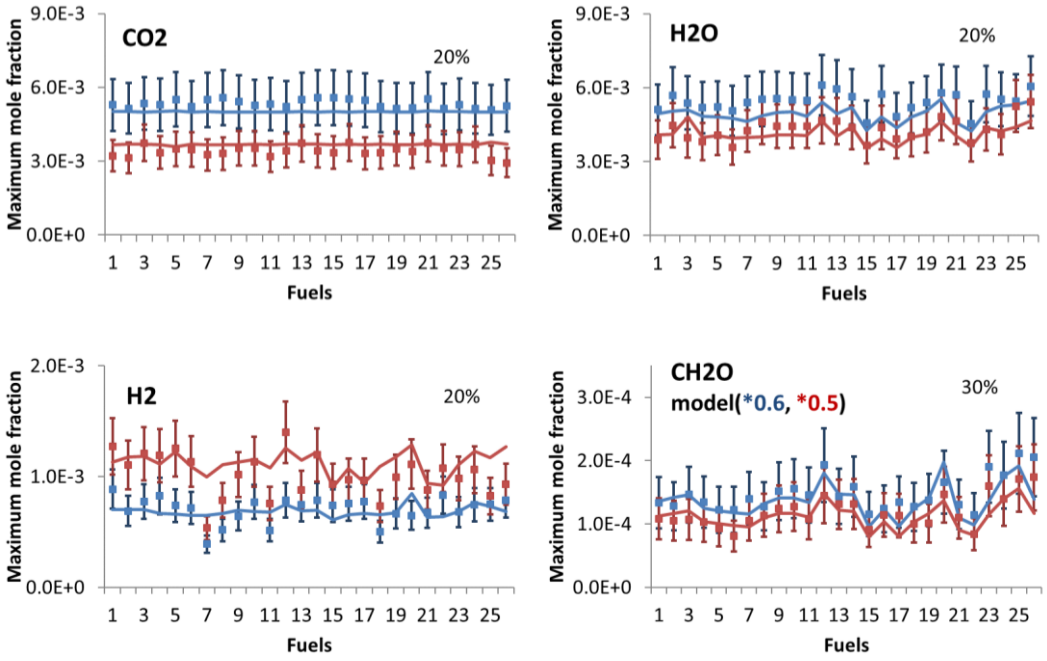

Fig. 8: Comparison of measured and predicted maximum mole fraction of O_2, major product species, H_2 and CH_2O of all fuels. Symbols: measurements, curves: model.

6.2 Intermediates – C_1-C_4

The comparison of modeled and measured CH_4, C_2H_2, C_2H_4, C_3H_6, C_4H_4, C_4H_6, and C_4H_8 for selected fuels formed during the combustion in the flow reactor is presented in Fig. 9. Most of these intermediates are predicted by the model within the uncertainty limits of the measurements. However, for some species, their formation by the model is seen at slightly lower temperatures compared to the measurements.

Comparing the five selected fuels, the amount of CH_4 is formed more in iso-paraffinic fuels compared to the n-paraffins and multicomponent fuels. In case of C_2H_2 and C_4H_6, nearly no variation in their concentration is seen to the fuel composition. For the fuel containing all five components, variation in the mole fraction of C_1-C_4 species is not large. Compared to them, the iso- and n-paraffinic fuels form these species by factor of 2 to 10 higher than fuels containing also cyclic components. In the figure the mole fractions are scaled to similar value for direct optical comparison. In general, the bulk of fuel component plays important role in the intermediate's formation. A figure depicting major formation routes of C_1-C_4 hydrocarbons, from fuel components, discussed here is provided in supplemental material.

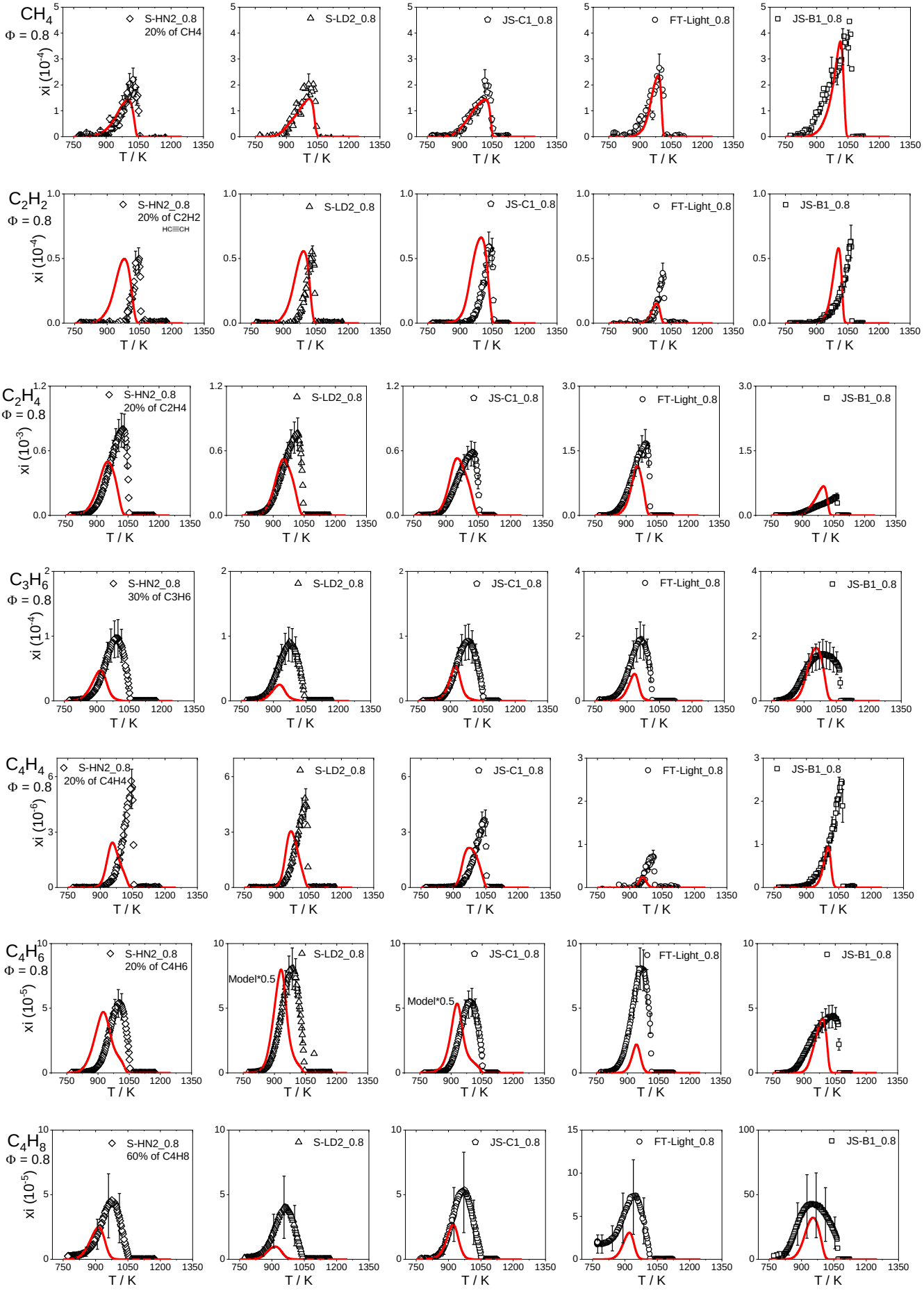
CH4
Φ = 0.8
S-HN2_0.8
20% of CH4
S-LD2_0.8
JS-C1_0.8
FT-Light_0.8
JS-B1_0.8
C2H2
20% of C2H2
HC≡CH
C2H4
20% of C2H4
C3H6
30% of C3H6
C4H4
20% of C4H4
C4H6
20% of C4H6
Model*0.5
C4H8
60% of C4H8
xi (10-4)
xi (10-3)
xi (10-5)
xi (10-6)
T / K

Fig. 9: Comparison of measured and predicted C_1-C_4 intermediates as a function of oven temperatures

Comparing all fuels, methane is mainly formed from H-abstraction reactions of fuel components by CH_3 radicals (Fig. 10). The variation in maximum concentrations at two stochiometry studied (Φ = 0.8 and 1.2) is not very large, at most 20%. Also the maximum CH_4 formed from different fuels vary within factor of 2 from each other. The measurement uncertainty of methane measurements are estimated to be about 20%. The model predictions of CH_4 are in good agreement and within the measurement uncertainty limits for most fuels. The variation of maximum CH_4 formed among the fuels is seen to be related to the total n- and iso-paraffin content of the fuel (Fig. 10). Here, the exception is S-LD2. This fuel contains 96% cyclic components, where the major source to CH_4 formation in modeled fuel is due to the presence of more than 50% decalin (highest among all fuels). The deviation of trend to n- and iso-paraffin is also seen in the measured fuel. Looking in to the fuel composition, among all Sasol fuels, only S-LD2 contains significant amount of tri-cycloparaffins (15 %m/m) which due to the absence in our model (as per our knowledge no reaction model of tri-cycloparaffin exist in literature) are lumped as bi-cycloparaffins i.e. decalin. The influence of tri-cycloparaffin to the methyl radical and thereby methane formation can be the reason for presented deviation. The only other fuel with significant amount of tri-cycloparaffin is JS-C1 containing 8 %m/m which also shows similar behavior as S-LD2. In general, except for the fuels containing >75% cyclic-compounds, the influence of non-cyclic components is visible in the CH_4 formation.

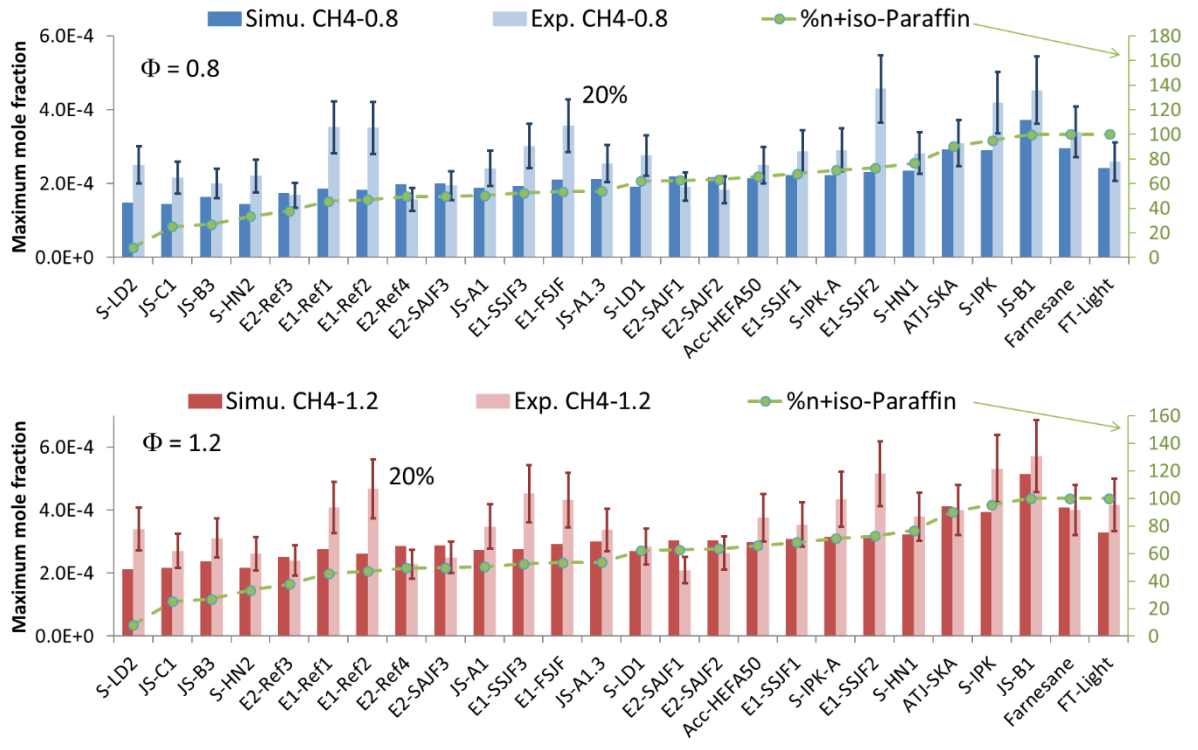

Fig. 10: Comparison of measured and predicted CH_4, maximum mole fraction of all fuels related with n- and iso-paraffinic content of the fuels.

The formation of acetylene, an important soot precursor, is well predicted by the model as shown in Fig. 11. The measurement uncertainties are estimated to be 20%. The main acetylene formation path in the n-paraffinic fuel and components is through the formation of butynyl (C_4H_5) radical from fuel radicals via olefin formation. Secondary channel could be from C_2H_3. The source of C_4H_5 radical in the fuels containing cyclic components (cyclo-paraffins, aromatics, cyclo-aromatics) are dominated mostly by cyclo-paraffins such as decalin, propylcyclohexane, where the ring opening of cyclic compound leads to the formation of C_5H_5 (cyclopentadienyl radical) → C_5H_5O (cyclopentadienoxy radical) → C_5H_4O (cyclopentadione) → C_4H_5 radicals. This route is also observed in the cyclo-aromatics such as indene or tetralin leading to acetylene formation. The total cyclic content of fuel can be related to both measured and modeled acetylene formation as seen in the Fig. 11. The exceptions are first five fuels in the plot, which are dominant iso-paraffinic fuels, which for obvious reason cannot be related to cyclic content. For these fuels, the main source of acetylene in addition to above described C_2H_3 is iso-butene (iC_4H_8) formed from the fuel radicals. The iso-butene formed reacts to form C_2H_2 from C_3H_4 through iC_4H_8 → iC_4H_7 → C_3H_4 → C_2H_2 channel.

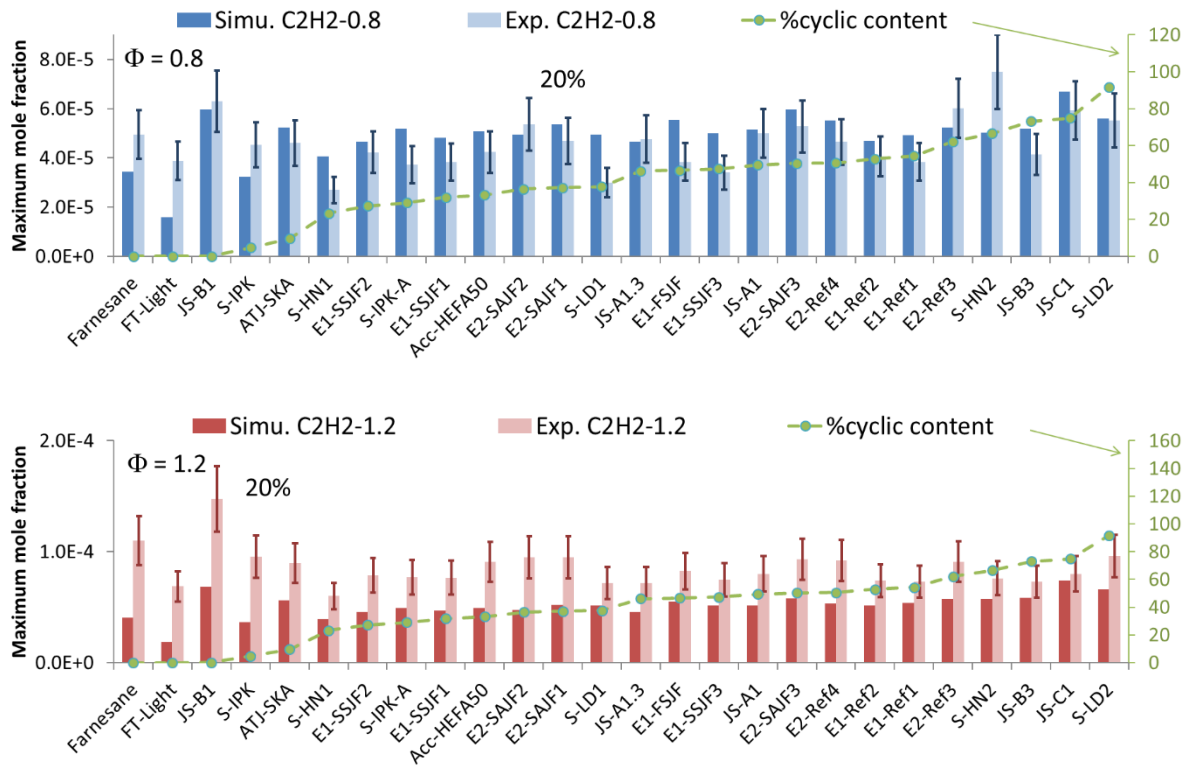

Fig. 11: Comparison of measured and predicted C_2H_2, maximum mole fraction of all fuels related with cyclic content (cyclo-paraffins + aromatics + cyclo-aromatics) of fuel.

The methyl radical recombination route to C_2H_6 is known and the methyl radicals can mainly be formed from fuel radical decompositions. The formation of C_2H_6 is underpredicted in model by factor of 3. The formation of C_2H_6 shows excellent relation with the total n-and iso-paraffin content of the fuel (Fig. 12). This relation is similar to methane formation which can be explained as both CH_4 and C_2H_6 are formed

from same source i.e. methyl radical. Only major deviation to this relation is seen in the measured S-LD2 which as specified earlier contains large amount of tri-cycloparaffins not included in the model, whose effect is unknown. A comparison of measurement with model is not possible for all fuels due to absence of measured data set for some fuels.

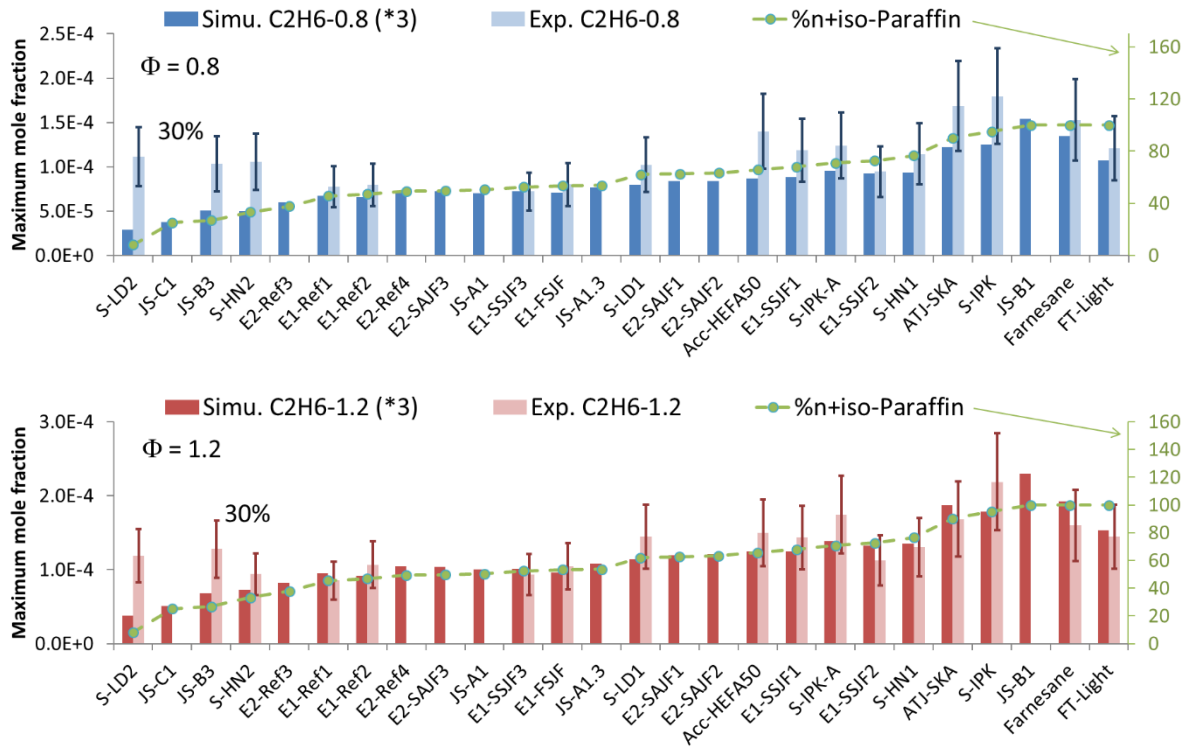

Fig. 12: Comparison of measured and predicted C_2H_6, maximum mole fraction of all fuels related with n- and iso-paraffinic content of fuel. Top plot shows only simulated data.

The stoichiometric variation in concentrations of olefins such as C_2H_4, C_3H_6, and C_4H_8 is largely not visible, where the experimental uncertainy is estimated to be 20-60% (Fig. 13). For these species the model predictions are in excellent agreement with the measurements, as seen in Fig. 13. In model, C_2H_4 is mainly formed from the paraffins (n-, iso-, and cyclo-paraffins) present in a fuel, C_3H_6 can additionally be formed from alkylbenzenes. The C_4H_8 are usually two isomers n- and i-C_4H_8 which are not resolved experimentally but both are present as separate species in the kinetic model. The model prediction shows n-C_4H_8 is mainly formed from either n- or iso-paraffins present in a fuel as well as from their branched intermediates whereas the source of i-C_4H_8 can be either n-/iso-paraffins or additionally in a minor channel from cyclo-paraffins. Fig. 13 shows that the C_2H_4 can be related to the n- and iso-paraffin whereas C_3H_6 can be related to iso-paraffins content of the fuel. The relation of n- and i-C_4H_8 is slightly complex with respect to fuels' composition. A weak trend in the formation of n-C_4H_8 is seen to be related to the n- or iso-paraffin content of the fuel whereas for i-C_4H_8 no clear trend is visible. The summation of C_4H_8 (n-C_4H_8 + i-C_4H_8 = $\sum C_4H_8$) predicted by the model is within the uncertainty limits of the measurements presented in Fig. 13.

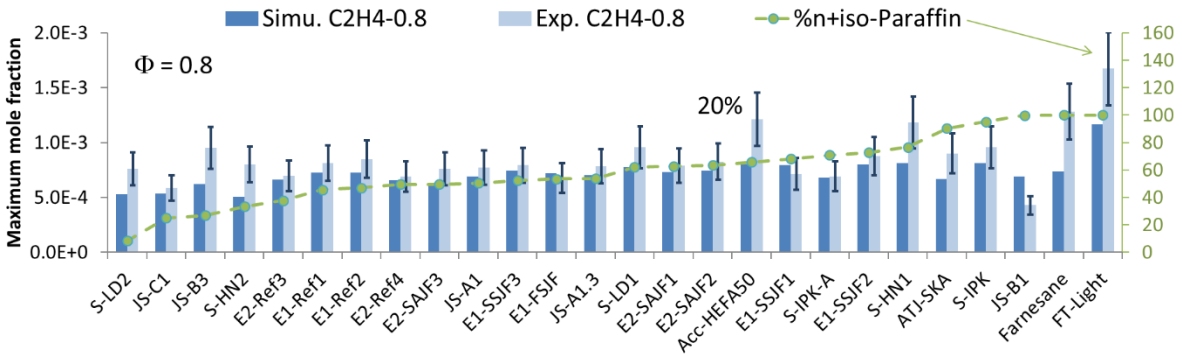
Simu. C2H4-0.8
Exp. C2H4-0.8
%n+iso-Paraffin
Maximum mole fraction
Φ = 0.8
20%
2.0E-3
1.5E-3
1.0E-3
5.0E-4
0.0E+0
160
140
120
100
80
60
40
20
0
S-LD2
JS-C1
JS-B3
S-HN2
E2-Ref3
E1-Ref1
E1-Ref2
E2-Ref4
E2-SAJF3
JS-A1
E1-SSJF3
E1-FSJF
JS-A1.3
S-LD1
E2-SAJF1
E2-SAJF2
Acc-HEFA50
E1-SSJF1
S-IPK-A
E1-SSJF2
S-HN1
ATJ-SKA
S-IPK
JS-B1
Farnesane
FT-Light

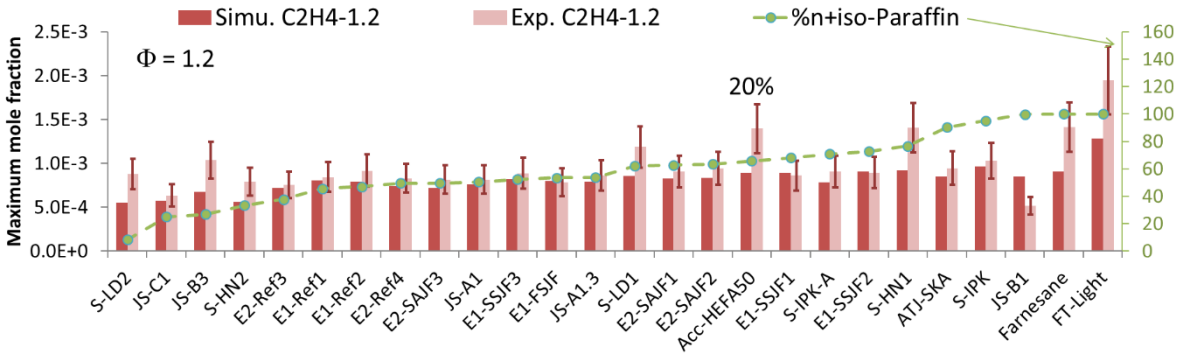
Simu. C2H4-1.2
Exp. C2H4-1.2
%n+iso-Paraffin
Maximum mole fraction
Φ = 1.2
20%
2.5E-3
2.0E-3
1.5E-3
1.0E-3
5.0E-4
0.0E+0
160
140
120
100
80
60
40
20
0
S-LD2
JS-C1
JS-B3
S-HN2
E2-Ref3
E1-Ref1
E1-Ref2
E2-Ref4
E2-SAJF3
JS-A1
E1-SSJF3
E1-FSJF
JS-A1.3
S-LD1
E2-SAJF1
E2-SAJF2
Acc-HEFA50
E1-SSJF1
S-IPK-A
E1-SSJF2
S-HN1
ATJ-SKA
S-IPK
JS-B1
Farnesane
FT-Light

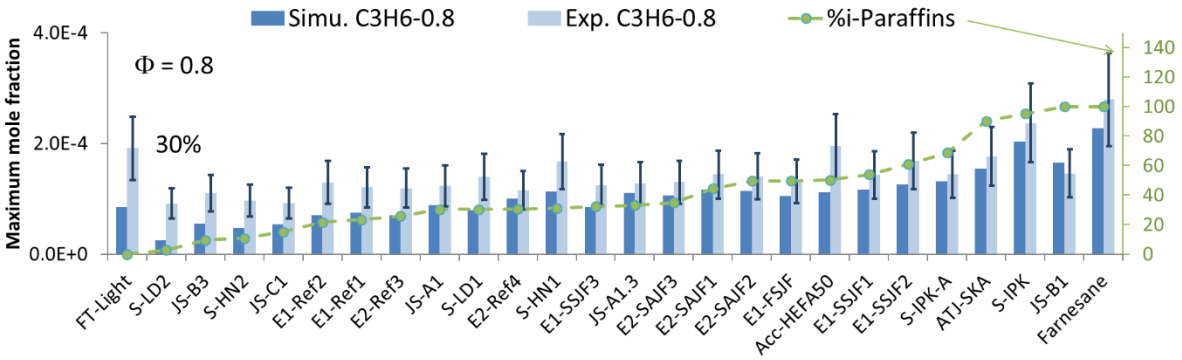
Simu. C3H6-0.8
Exp. C3H6-0.8
%i-Paraffins
Maximum mole fraction
Φ = 0.8
30%
4.0E-4
2.0E-4
0.0E+0
140
120
100
80
60
40
20
0
FT-Light
S-LD2
JS-B3
S-HN2
JS-C1
E1-Ref2
E1-Ref1
E2-Ref3
JS-A1
S-LD1
E2-Ref4
S-HN1
E1-SSJF3
JS-A1.3
E2-SAJF3
E2-SAJF1
E2-SAJF2
E1-FSJF
Acc-HEFA50
E1-SSJF1
E1-SSJF2
S-IPK-A
ATJ-SKA
S-IPK
JS-B1
Farnesane

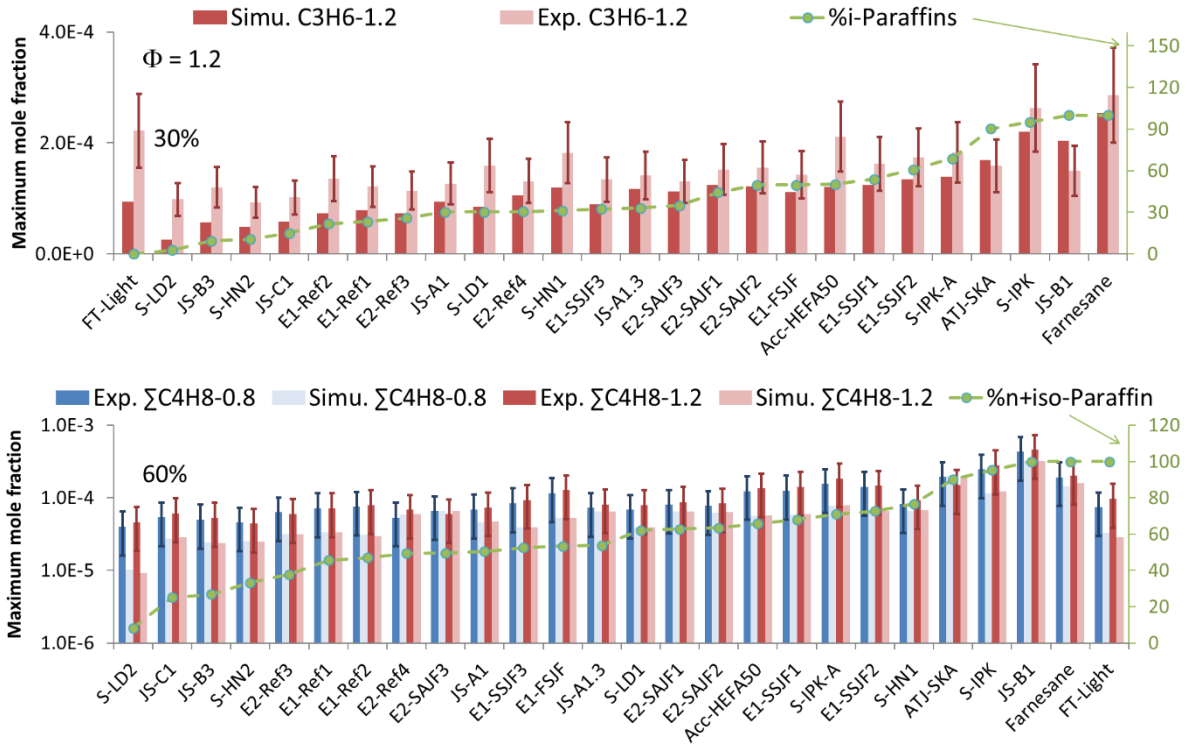

Fig. 13: Comparison of measured and predicted C_2H_4, C_3H_6 and $\sum C_4H_8$ maximum mole fraction of all fuels.

The formation of vinyl-acetylene (C_4H_4) is dominated from tetralin, decalin or n-propylbenzene in the modeled fuels (Fig. 14). This is found to be related to the cyclic content of the fuel. The cyclo-paraffins present in a fuel mixture are responsible for the formation of butadiene (C_4H_6), which is visible in its relation to cyclo-paraffinic content of fuel. Both these species can be measured within 20% precision. The exception to this relation in both species is mainly iso-paraffinic fuels for obvious reason, where the formation of C_4H_6 is possible through iso-paraffinic fuel radicals. The model prediction of C_4H_4 is about 1.5 times lower than the measurements whereas most of the C_4H_6 are predicted within the experimental error limits.

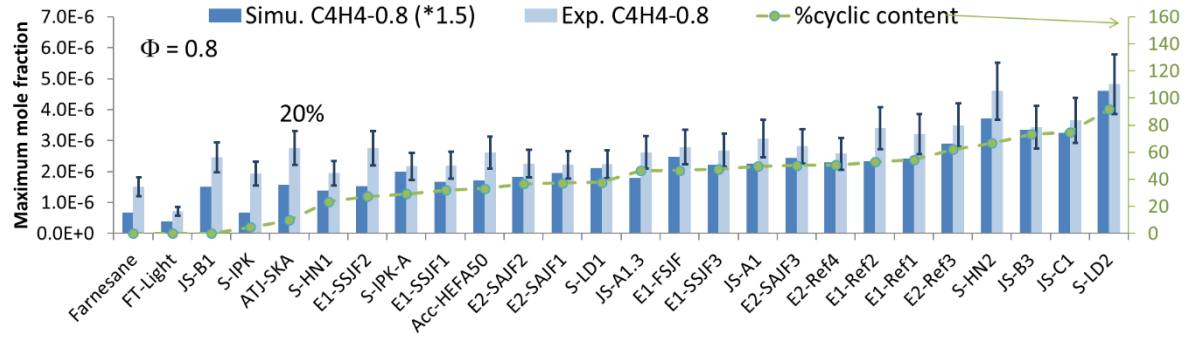

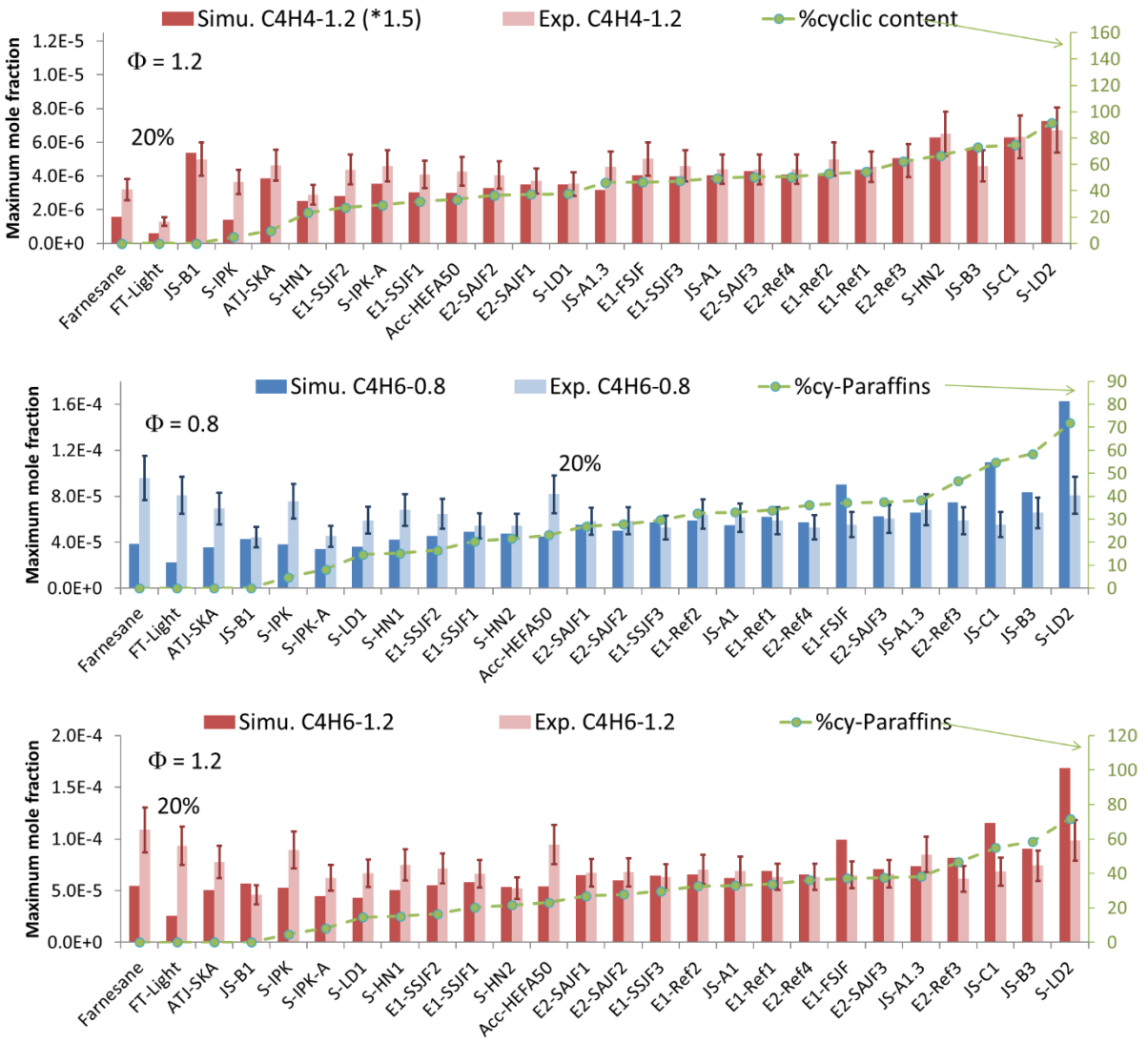

Fig. 14: Comparison of measured and predicted C_4H_4, and C_4H_6, maximum mole fraction of all fuels.

In general, the trends in C_1-C_4 intermediates are seen related to n- and iso-paraffins or total cyclic content of the fuel in most of the above studied cases, except for the fuels containing mainly iso-paraffins (<90%). The exception in latter case is due to the fact that, they behave more similar to cyclic containing fuels however are excluded from the relation due to their apparent absence.

Overall the surrogate strategy together with the chemical kinetic model are in excellent agreement with the experimental data. The accurate prediction of C_1-C_4 species will help to evaluate some soot formation precursors as well as influences on (prompt) NO (via CH, which is dependent on hydrocarbon chemistry). The model as well as the strategy leave room for improvement in the future. For a small number of species, the systematic error between model and experiments, shows the potential of improving the chemical kinetic model. The scatter of the non-systematic error between model and experiments could be reduced by replacing specific compounds with other compounds of the same class for selected fuels in the future.

6.3 Intermediates – Aromatics

The soot precursors such as single-ring benzene, double-ring indene, naphthalene, biphenyl as well as triple-ring acenaphthylene and phenanthrene formed during the combustion in the flow reactor are discussed here for the studied fuels.

For a better overview, the reaction paths of different aromatic species formed from fuel components during the combustion of the fuels are shown in the Fig. 15. The rate of production (ROP) is depicted at about 50% of fuel conversion and shows only major reaction routes dominant at the present conditions. At intermediate temperature ranges fuels, containing mainly n- and iso-paraffins, form benzene from C_2 and C_4 species however at the high flame temperatures the propargyl recombination route is dominant (for detailed discussion see [29]). However, in presence of cyclic fuel components, the formation of benzene from n-/iso-paraffin route is negligible, due to the predominant formation of benzene from the cyclic fuel component itself (see Fig. 16). The benzene formation routes from cyclo-paraffins and in aromatics are identical at intermediate and high temperatures. The fuels studied in this work vary by their selection of the surrogate components and by their amount. Thus, the soot precursor formed can have multiple formation routes as it is discussed in this section and shown in Fig. 15. In such case, the influence and ranking of each individual component on the benzene formation is not straightforward as the molecular structure of cyclic compound and its amount both play an important role. Therefore, a generalization from the reaction routes is challenging.

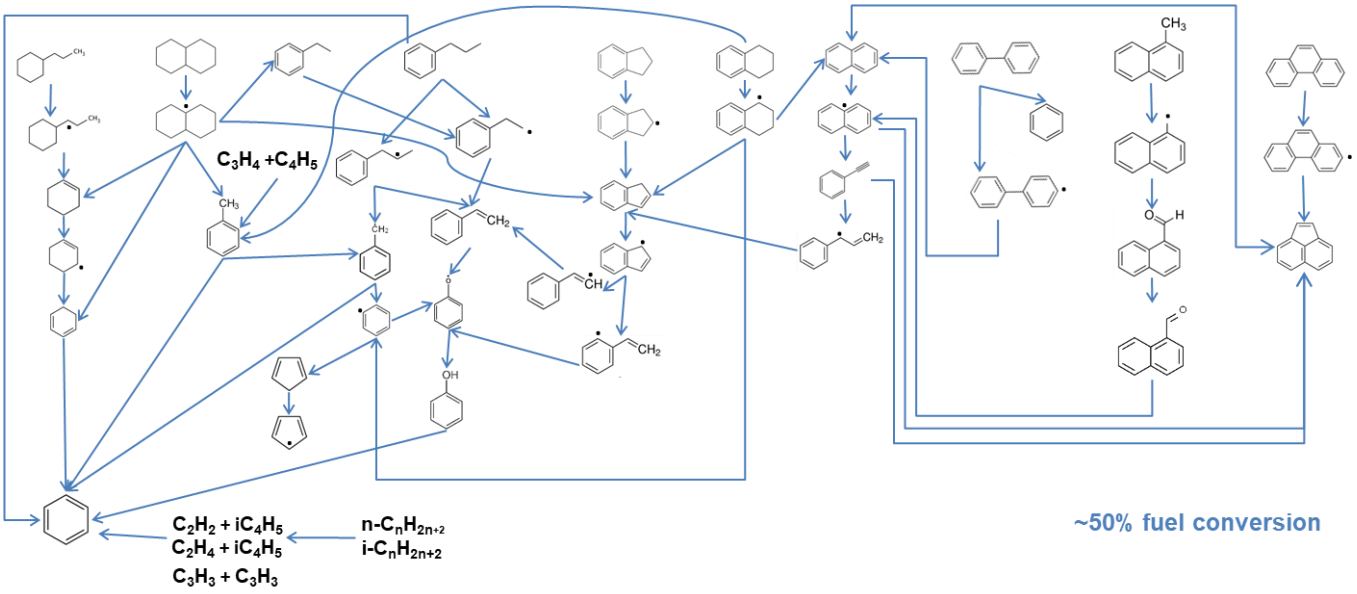

Fig. 15: Rate of production analysis at 50% fuel conversion. Only main routes are shown, specific individual reactions may be missing.

1-ring aromatic

In Fig. 16, the formation of benzene (C_6H_6) is slightly higher for S-LD2 (cyclo-paraffinic case) than found in S-HN2 (mono-aromatic case) and JS-C1 (di-aromatic case). The fuel S-LD2 contains the

highest amount of cyclo-paraffins and total cyclic compounds (Fig. 1) which is 20% higher than the next two fuels S-HN2 and JS-C1 and is exactly reflected in benzene concentration. Although both S-HN2 and JS-C1 contain diverse compositions of mono- and di-aromatics they produce nearly same amount of benzene. This is because either propylbenzene or similar mono-aromatics and decalin present in a fuel are mainly responsible for the benzene formation and more stable di-aromatics have a lower tendency to break down and form lower aromatics. The benzene concentrations, for JS-B1 and FT-Light containing iso- and n-paraffins respectively, are apparently low compared to other fuels, due to the formation paths via C_2-C_4 species. However, iso-paraffins (JS-B1) lead higher amounts of benzene formed compared to FT-Light, as branched molecules have a higher likelihood to form cyclic structures.

The formation trends of toluene (C_7H_8) as shown in Fig. 16 are similar to the ones of the benzene formation. In fuel containing cyclic compounds, modeled toluene is formed at slightly earlier temperature than found in the measurements. The major sources of toluene in fuels containing cyclic components are decalin or tetralin present or formed in fuel as seen in Fig. 15.

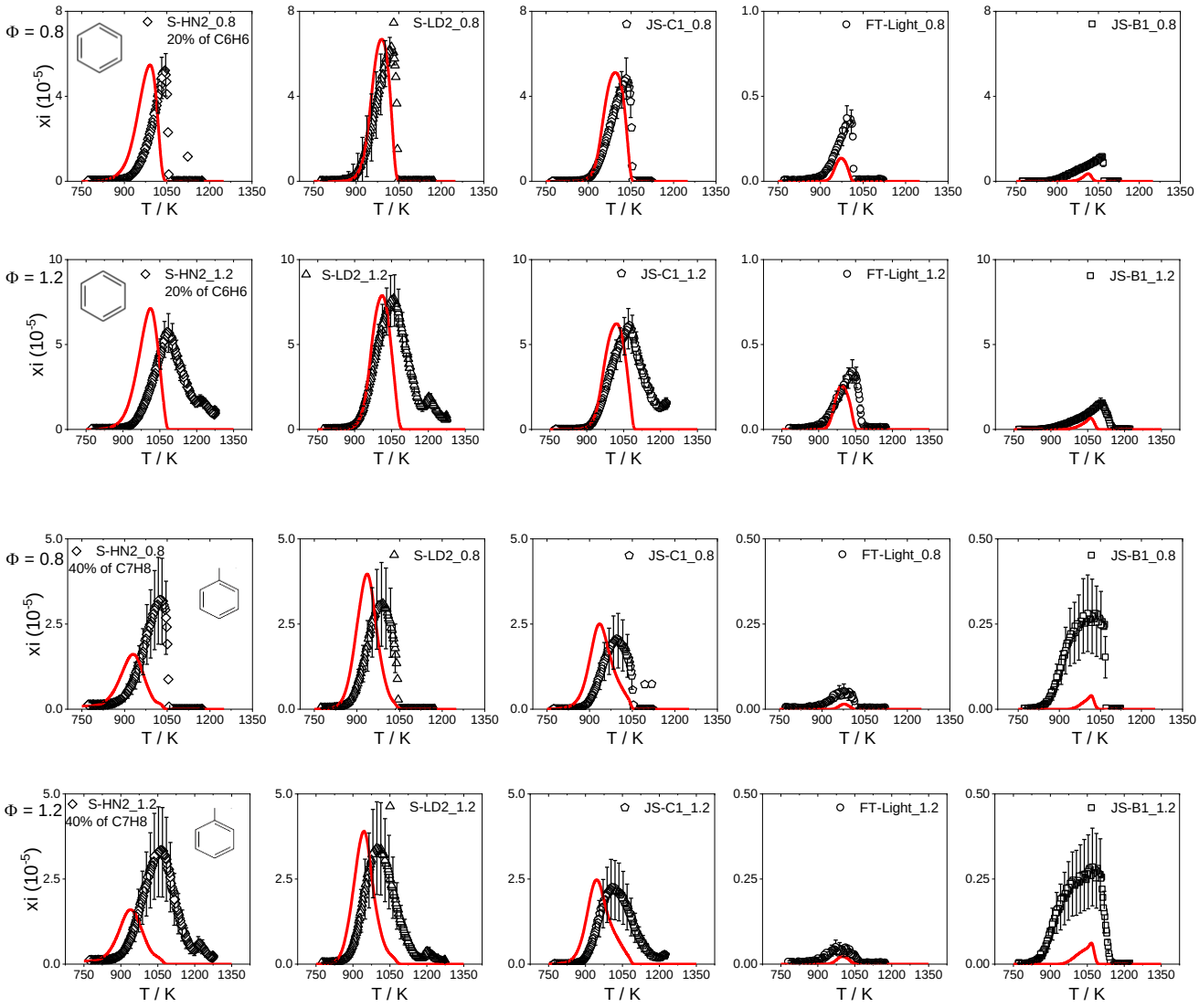

Fig. 16: Comparison of measured and predicted C_6H_6 and C_7H_8 as a function of oven temperatures.

The comparison of selected fuels showed that different aromatic intermediates are responsible for the formation of larger PAH species. When looking at multicomponent fuels, it is important to understand the effects of the single components on the soot precursor formations to deeply evaluate soot formation potentials. For example, the naphthalene produced from tetralin or methylnaphthalene is about 3 to 4 orders of magnitude higher than that found in n-/iso-paraffins. Most of the aviation fuels can be mainly comprised of n-/iso-paraffins (50-70%); the potential of soot precursor formation mainly lies in the amount of cyclo-paraffins and aromatic contents of fuels (usually <20%).

In order to generalize the analysis of soot precursor formations, we use the index of hydrogen deficiency (IHD) to represent each fuel. For a hydrocarbon C_xH_y, index hydrogen deficiency (IHD) is defined as IHD = (x+1)-(y/2) which represents the number of unsaturation and cyclic structure present in a hydrocarbon. Detailed discussion on IHD and its relation to hydrocarbons can be found in our previous work [39, 28]. A linear relation between IHD and hydrogen content of the fuels can be stated for jet fuels since their mean molar mass is not seen to differ significantly. The use of the IHD of complex fuels is separating the saturated components such as n- and iso-paraffins (IHD = 0) that have a lower potential forming soot precursors, compared to cyclic or aromatic paraffins. Thereby, the use of the IHD is beneficial for the evaluation of the formation of intermediates or soot precursors, as it reduces the degrees of freedom in the analysis [39]. It should be noted that the IHD of fuel and fuel surrogate may vary slightly due to difference in individual components considered.

As discussed in our previous work on three n-alkanes [29], the major formation paths to benzene formation in n-paraffins are through even (C_2 + C_4) route. These reaction routes are also found to extend to iso-paraffins such as iso-octane (discussed in [19]) as well as farnesane containing tertiary and quaternary carbons. Compared to them, the formation paths of benzene in fuels containing cyclic compounds vary significantly and depend on their individual structure. The cyclo-paraffins, both mono and di, such as cyclohexane (discussed in [19]), propylcyclohexane, and decalin show similar production routes for benzene, namely through decomposition of cyC_6H_7 which can be formed from chemical cascading of cyC_6H_{10} formed from first fuel radicals of respective cyclo-paraffinic fuels. Compared to them, C_6H_6 is directly formed from fuel decomposition in aromatics such as n-propylbenzene. The cyclo-aromatic fuels such as tetralin and di-aromatic fuel methylnaphthalene are more stable and are not directly responsible for benzene formation. In these fuels, benzene is formed from intermediates toluene or benzyl radical and including minor channel of C_2 + C_4 route. Considering these neat components, the benzene concentrations increases (shown in Fig. 17) generally (not strictly) in the order n-paraffins < iso-paraffins < mono-cyclo-paraffins < di-cyclo-paraffins < mono-aromatics > di-aromatics. The di-aromatics can lead to lower amount of mono-aromatics due to their molecular stability. Thus, the complex molecular structures lead to different production routes among different molecular classes but are quite similar within a given class, unlike production routes of aromatics which can be more diverse.

In a complex fuel mixture, as we reported earlier, minor amounts of specific component classes can have major impacts on the fuel sooting tendencies [39]. Fig. 17 shows the comparison of measured and modeled peak benzene mole fraction of fuels (Fig. 17 (right)) along with neat components (Fig. 17 (left)). The fuels studied in this work show linear increase in benzene formation although the benzene formation decreases for bicyclic aromatics (IHD of 4 and 5, Fig. 17 (left)).

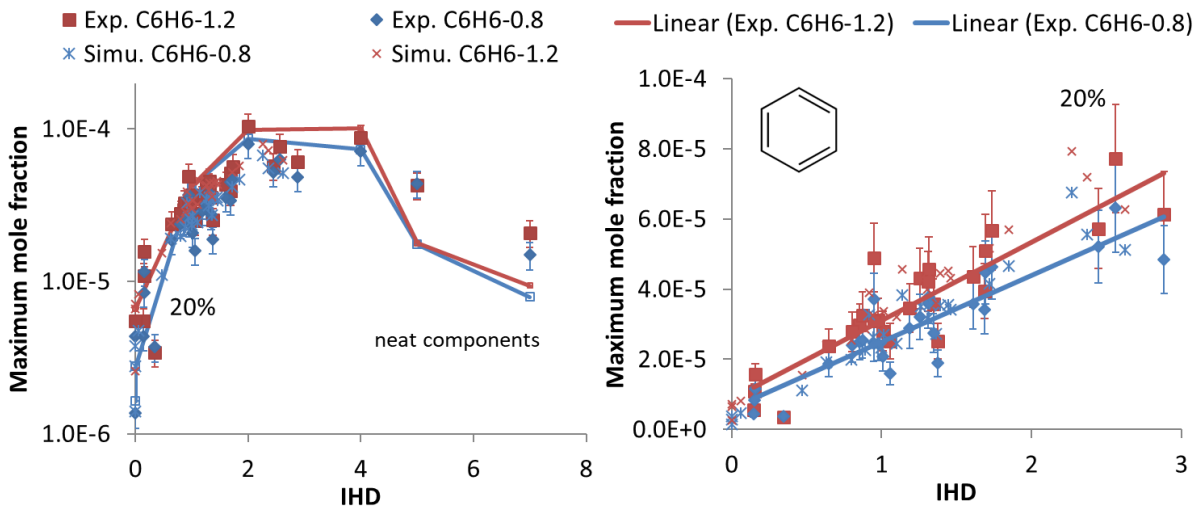

Fig. 17: Comparison of measured and predicted C_6H_6 maximum mole fraction of all fuels and neat components as a function of their IHD.

Similar trend can be seen for the formation of toluene presented in Fig. 18. Toluene is known to be formed from benzene, but in the present fuels its formation is dominated from the decalin or tetralin radical decomposition (Fig. 18). In the modeled fuels, the maximum mole fractions are excellently reproduced by the model as shown in Fig. 18. The maximum concentration of toluene formed is independent of the studied fuel stoichiometry and for the fuels investigated their concentrations are within factor of two except for iso-paraffinic fuel JS-B1 where no decalin is present. For fuel JS-B1 which is mainly iso-paraffinic, its formation is resulting from the reaction of the iC_4H_5 radical with C_3H_4 and its concentration is an order of magnitude lower compared to other fuels. For the studied neat components, di-aromatics form slightly less toluene compared to mono-aromatics. In general, maximum mole fractions of toluene increase in fuels with increasing IHD.

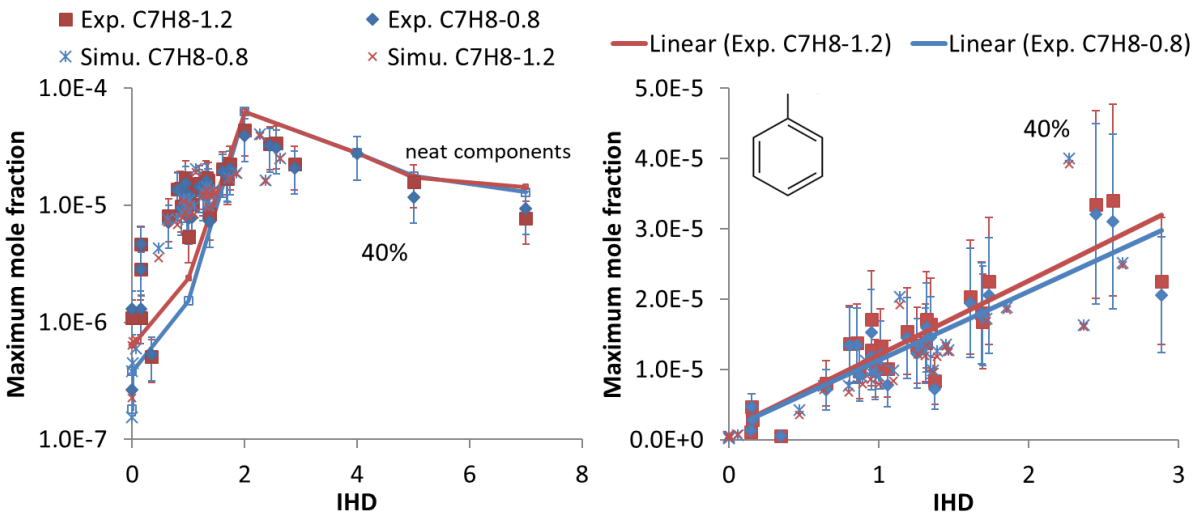

Fig. 18: Comparison of measured and predicted C_7H_8 maximum mole fraction of all fuels and neat components as a function of their IHD.

Similar findings were reported by Corporan et al. [62] who studied the impact of fuel composition on selectivity of intermediates measured in a swirl combustor exhaust. Their data showed fuels consisting of predominantly n-paraffinic components, produces very low levels of benzene and toluene. Whereas the fuels with significant iso- and cyclo-paraffin content produce both of these intermediates, mostly linearly to their amount – slightly higher benzene to toluene. They compared their data to Jet A which showed the ratio of benzene to toluene to be close to one. The comparison of maximum benzene and toluene formed during the combustion with our data shows similar trends. Fig. 19 shows this comparison of our data for neat components as well as for fuels, both measured and modeled. The figure is color coded with A to D cases (see section 4.1) for better visualization. The dominant n-paraffinic fuel FT-Light and n-decane form the lowest amounts of both these species. All the iso-paraffinic fuels categorized under A form higher amounts of these species but still lower than other categories (B, C, and D) containing cyclic compounds (categorization as in Fig. 1). A linear increase in benzene to toluene formation is seen with the increase in aromatic content in the fuel, with ratio more lent to the benzene side. Among neat components one observes that propylcyclohexane, n-propylbenzene, and decalin, produce more benzene compared to toluene; methylnaphthalene and tetralin in comparison form more toluene compared to benzene. However, very few of the reference fuels show benzene to toluene ratios close to one, either experimentally or in modeling, as observed by Corporan et al. [62]. This deviation is comprehensible as their concentrations in exhaust gas of a turbulent combustor are beyond the peak concentrations compared to our measurement in a laminar combustion zone.

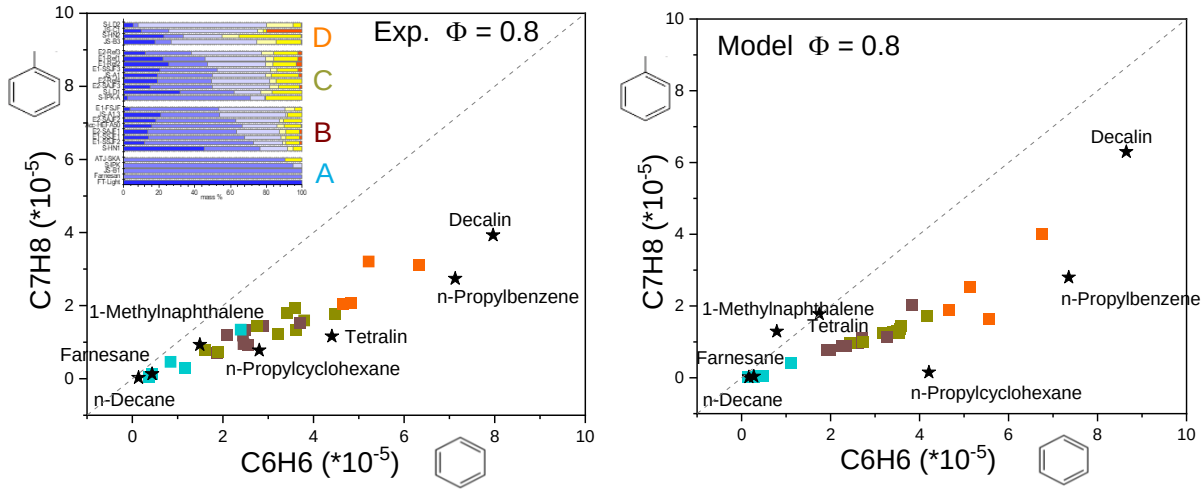

Fig. 19: Impact of fuel component on selectivity on benzene and toluene formed. Both measured (left) and modeled (right) maximum toluene mole fraction are plotted against maximum benzene mole fractions. The fuels' data points are color coded by its composition categorized by A to D as in Fig. 1.

2-ring aromatic

The influence of the diversity in fuel-bound aromatics is more visible in the concentrations of larger aromatics formed during fuel combustion. The fuel S-HN2 containing the largest mono-aromatics forms indene (C_9H_8) followed by S-LD2 and JS-C1 (Fig. 20). The formation pathways or source of indene depends on the surrogate components e.g. in S-HN2 indene is formed due to the presence of indane as fuel component, whereas in JS-C1 indene is formed from decalin and in S-LD2 in addition to decalin also from tetralin radicals. Compared to them, a minor amount of indene is formed in JS-B1 from fuel bound iso-paraffins and none in n-paraffinic fuel FT-Light. Thus, bicyclic-paraffins or fused cyclo-aromatics are seen to be precursors to the indene formation.

The highest amount of bicyclic aromatic naphthalene ($C_{10}H_8$) is formed in JS-C1 which also contains the highest amount of di-aromatics (Fig. 20). The major source of naphthalene, as shown in Fig. 15, is tetralin (considered as mono-aromatics in surrogate) as well as methylnaphthalene. For both S-HN2 and S-LD2, it is formed from tetralin, where the relative amount of tetralin in S-LD2 is slightly higher, also reflected in the naphthalene formation. The naphthalene found in JS-B1 and FT-Light is negligible.

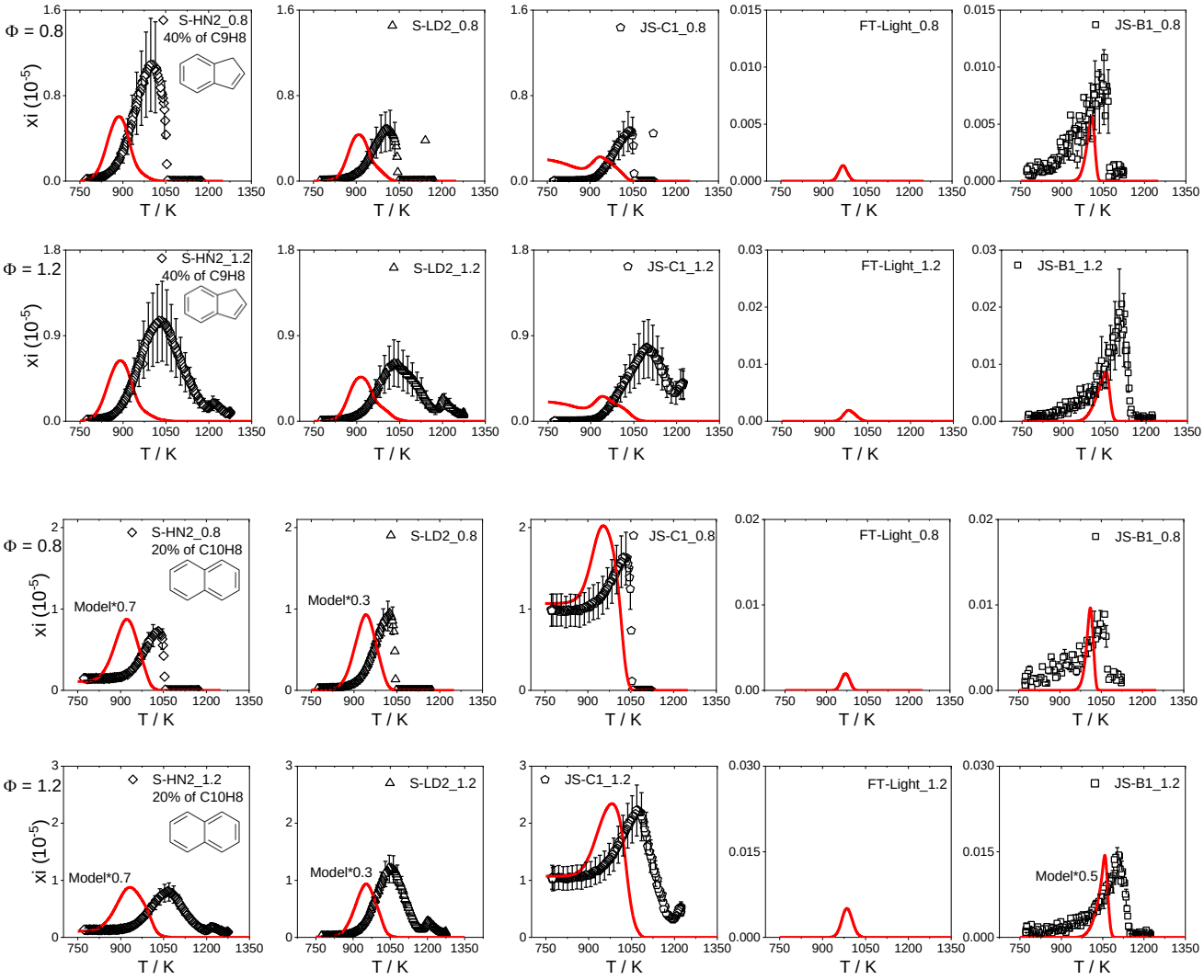

Fig. 20: Comparison of measured and predicted indene (C_9H_8) and naphthalene ($C_{10}H_8$) as a function of oven temperatures.

Significant amounts of indene can be formed during the combustion of fuels containing cyclic compounds compared to n- and iso-paraffins. The fuel precursors leading to their formation are indane, tetralin or decalin where their first fuel radicals lead directly to the indene formation. In neat components, indene mole fractions increase with increasing IHD from n-paraffins to mono-aromatics (Fig. 21). Similarly, as seen for benzene production in Fig. 19, di-aromatics produce less indene due to their tendency to grow further in their molecular structure rather than breaking down to smaller species.

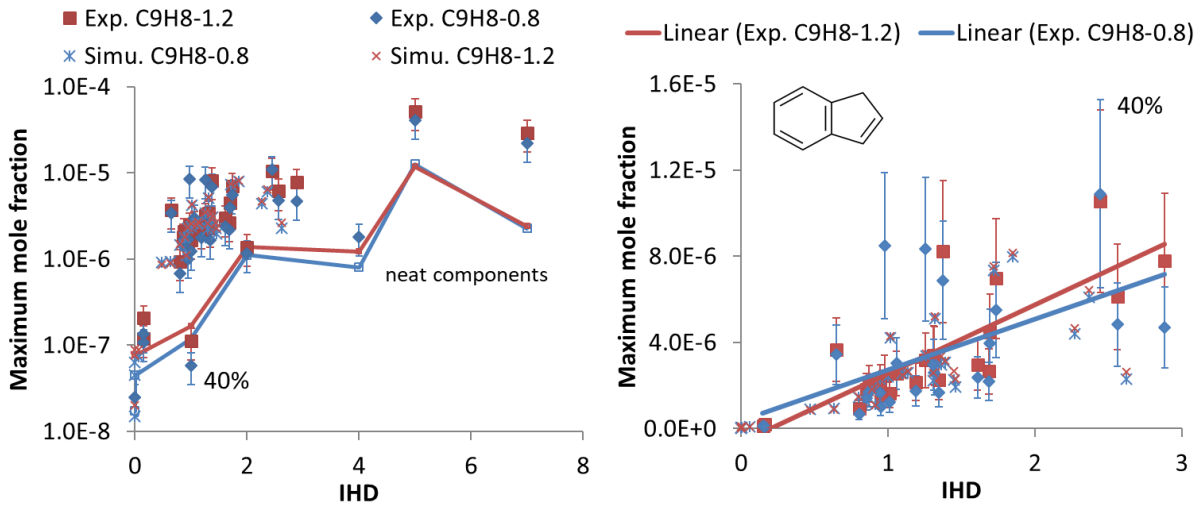

Fig. 21: Comparison of measured and predicted C_9H_8 maximum mole fraction of all fuels and neat components as a function of their IHD

In the present work, indene and other aromatics species are formed in the temperature range of 800-1100 K. The thermal decomposition of indene is initiated through abstraction of H-Atom from C-H bond in the C_5-ring forming resonantly stable indenyl radical at intermediate temperatures [63]. As presented in Fig. 22, the recombination of indenyl radicals or combination between indene and indenyl radicals lead to the formation of four-ring aromatic hydrocarbon such as $C_{18}H_{12}$ (chrysene) and $C_{18}H_{10}$ (benzo(ghi)fluoranthene). Other important larger aromatics are formed from the reactions of indenyl: (i) with methyl to form $C_{10}H_8$ (naphthalene), (ii) with C_5H_5 forming $C_{14}H_{10}$ (phenanthrene), (iii) forming phenyl-acetylene leading to the subsequent formations of $C_{12}H_8$ (acenaphthylene) as well as the five-ring aromatic $C_{20}H_{12}$ (benzo(a)pyrene). Thus, indene is an important intermediate leading to further growth of many larger aromatic products. As shown in Fig. 21, the modeling trends of the maximum indene mole fractions are in good agreement with the experimental results.

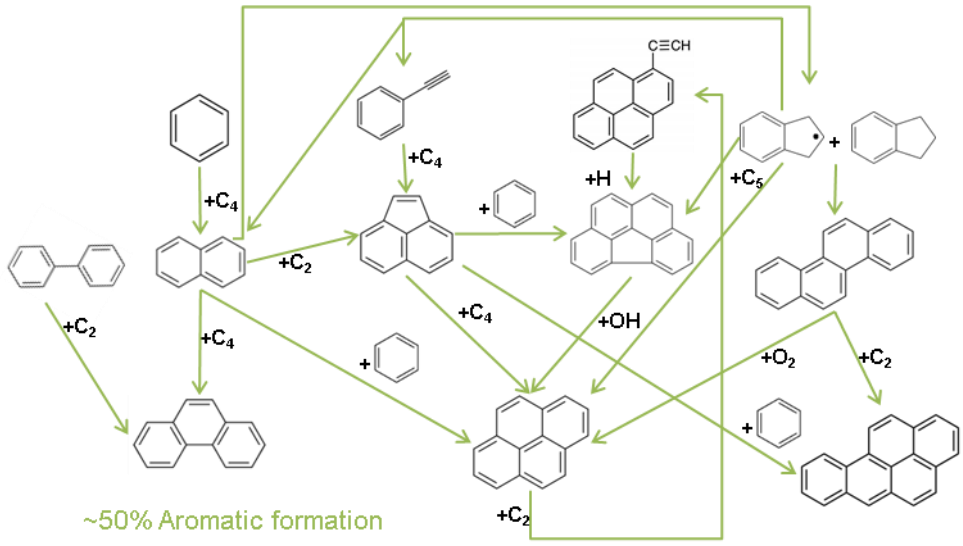

Fig. 22: Formation route of larger polycyclic hydrocarbons with indene, indenyl radical and acenaphthylene playing central role.

Naphthalene is present in some fuel surrogates as a fuel component and is formed as well during fuel oxidation. Compared to the measurements, the modeled naphthalene concentrations for all fuels are well reproduced (Fig. 23). As seen earlier, naphthalene can be formed from indenyl radical, which itself can be formed from decalin, tetralin as well as indene and indane. This is visible in the Fig. 23 where in neat components naphthalene formation increases with IHD, except for propylbenzene (IHD = 4). Similar to the behavior of the indenyl radical, propylbenzene readily decomposes to benzene, rather than immediately forming larger aromatics. For the fuels studied, in general, with the increase of the IHD, the amount of naphthalene increases. The maximum mole fractions of naphthalene are over-predicted by the model roughly by factor of 2 (Fig. 23).

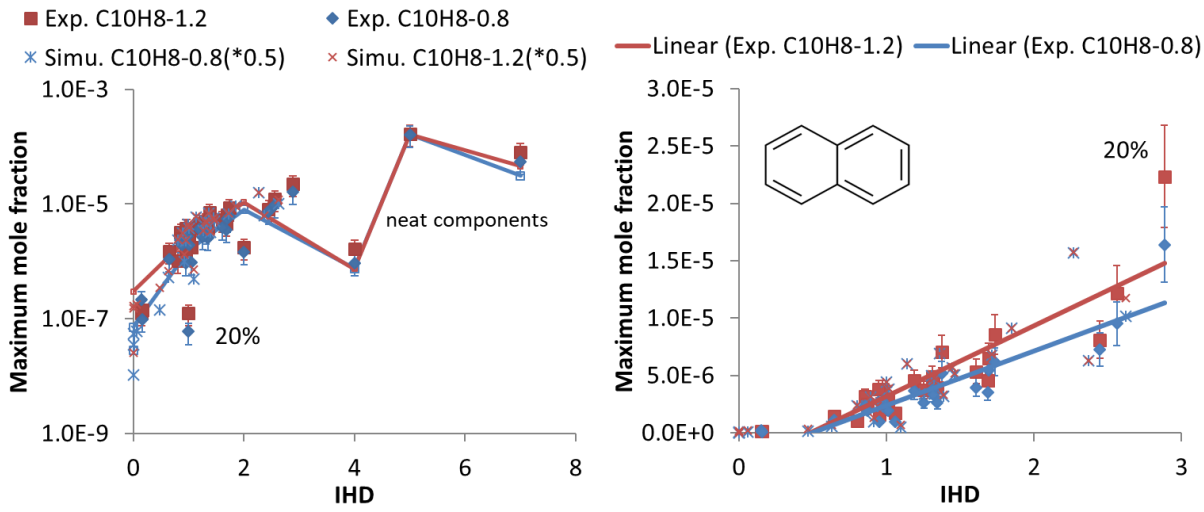

Fig. 23: Comparison of measured and predicted $C_{10}H_8$ maximum mole fraction of all fuels and neat components as a function of their IHD.

Very low amounts of $C_{12}H_{10}$ are formed for the fuels and components presented at our conditions. Here the measurement uncertainty can be up to 40%. The predictions of $C_{12}H_{10}$, considered as biphenyl in model, are twenty times lower than the measurements as shown in Fig. 24. In the model, the reactions responsible for the biphenyl formation are mainly phenyl addition reactions to benzene.

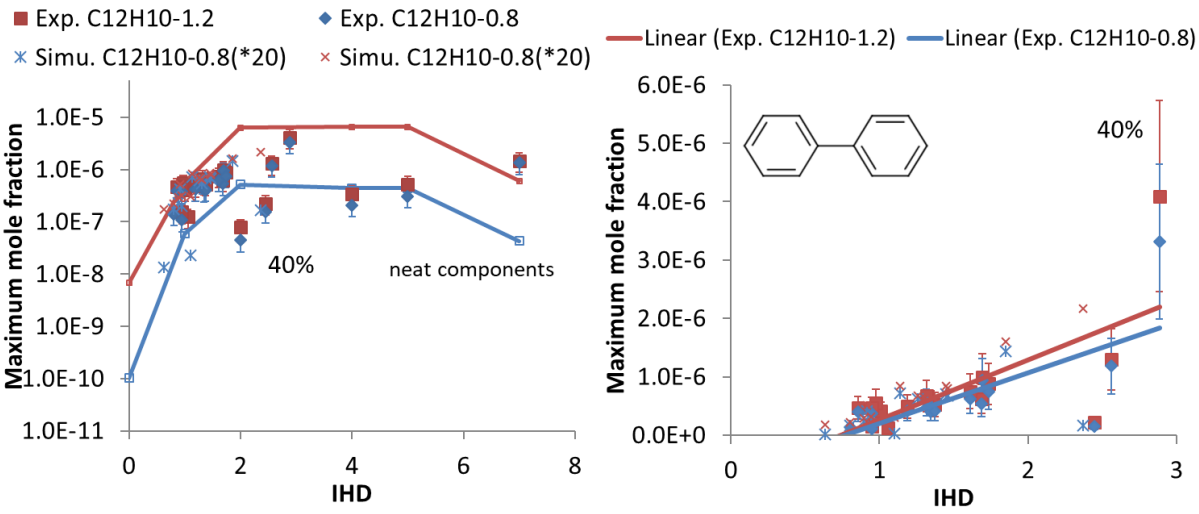

Fig. 24: Comparison of measured and predicted $C_{12}H_{10}$ maximum mole fraction of all fuels and neat components as a function of their IHD

3-ring aromatic

Ethynyl-naphthalene and acenaphthylene are available in the kinetic model as the $C_{12}H_8$ species. A summation of these both species is considered in comparison with the measured $C_{12}H_8$ profiles. As shown in Fig. 15, acenaphthylene ($C_{12}H_8$) is mainly formed from phenanthrene if present as a fuel component. At higher temperature, it can be also formed from phenyl-acetylene or naphthalene. Phenyl-acetylene is usually formed from indenyl radicals which can be formed from indene, indane or tetralin whereas naphthalene can be present as a fuel component or can be formed from tetralin.

Finally, Fig. 25 shows that multi-ring aromatics are not formed in the n- or iso-paraffinic fuels (JS-B1 and FT-Light) due to negligible concentration of intermediates forming them. For the three fuels containing cyclic compounds in Fig. 25, similar amounts of $C_{12}H_8$ are formed in JS-C1 and S-LD2, whereas for S-HN2 it is formed less by about a factor of three compared to the other two fuels. Large amounts of di-aromatics are present as fuel component in JS-C1 compared to S-LD2. However, both JS-C1 and S-LD2 form equal amount of $C_{12}H_8$. This is due to the different selectivity of different aromatics towards their formation. The significant source of $C_{12}H_8$ in S-LD2 is the phenanthrene which is absent in JS-C1. However, in JS-C1, the formation of $C_{12}H_8$ is due to the presence of a higher amount of tetralin compared to JS-C1. Here the tetralin leads to the $C_{12}H_8$ via formation of naphthyl radical.

Although both fuels form the same amount of $C_{12}H_8$, their precursor sources differ. In S-HN2, the $C_{12}H_8$ is formed from phenyl-acetylene, which itself is formed from indene.

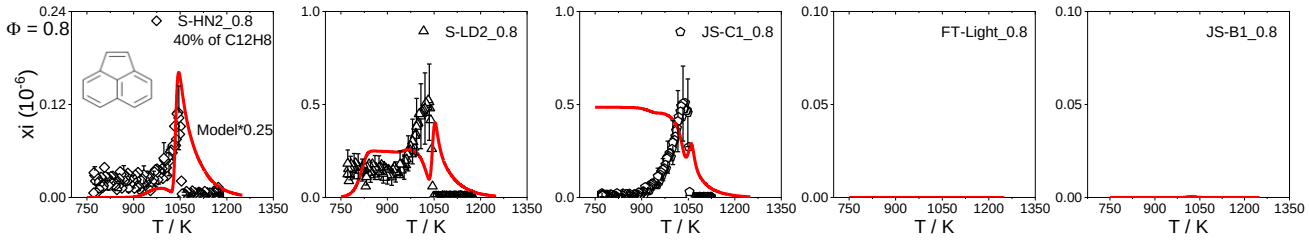

Fig. 25: Comparison of measured and predicted acenaphthylene ($C_{12}H_8$) as a function of oven temperatures.

The major contribution to the total $C_{12}H_8$ is mainly from acenaphthylene in the model. In some fuel surrogates acenaphthylene is present as fuel component (e.g. JS-C1). Although the measurement uncertainty can be up to 40% the model experiment comparison is exceptionally well (Fig. 26). The formation of $C_{12}H_8$ is mainly dominated by the presence of fused cyclo-aromatics rings such as tetralin, indane, or indene present in a fuel that form the $C_{12}H_8$ precursor indenyl. Propargyl addition to indenyl can also lead to $C_{12}H_8$ formation, which may be less important at the intermediate temperatures of our flow reactor where usually propargyl concentrations are low [29]. An additional path usually observed at flow reactor temperatures is the cyclization of phenyl-acetylene ($A1C_2H$) by di-acetylene (C_4H_2) leading to $C_{12}H_8$ (Fig. 22).

Another 3-ring aromatic present as fuel component is $C_{14}H_{10}$. In model only phenanthrene is present and compared to the measured $C_{14}H_{10}$ (Fig. 26). The formation route of phenanthrene is mainly from 2-ring naphthalene or biphenyl through addition of C_4 and C_2 component respectively (Fig. 15). The model underpredicts its formation by order of 2 compared to the measurements.

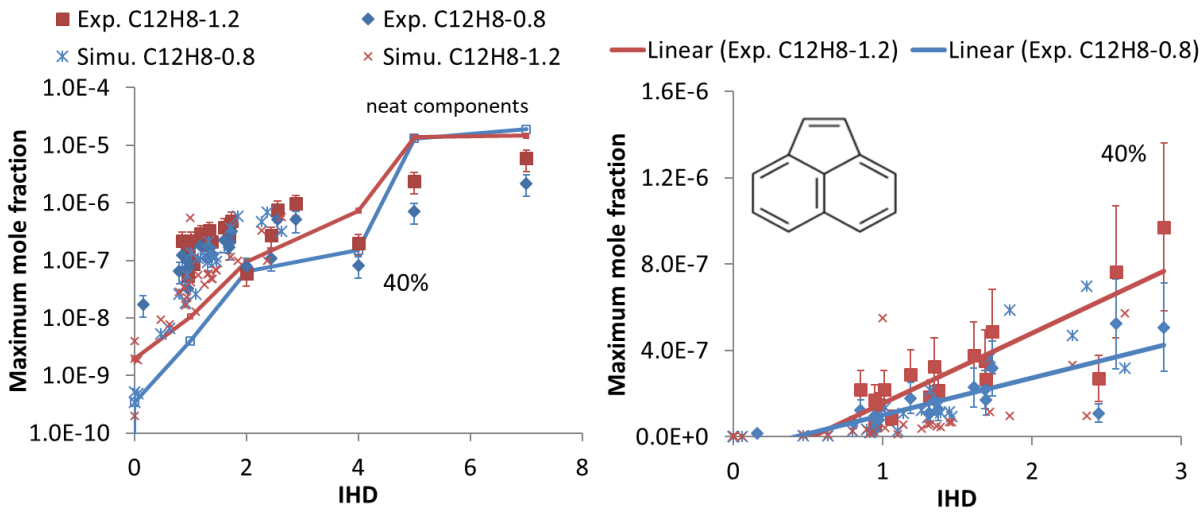

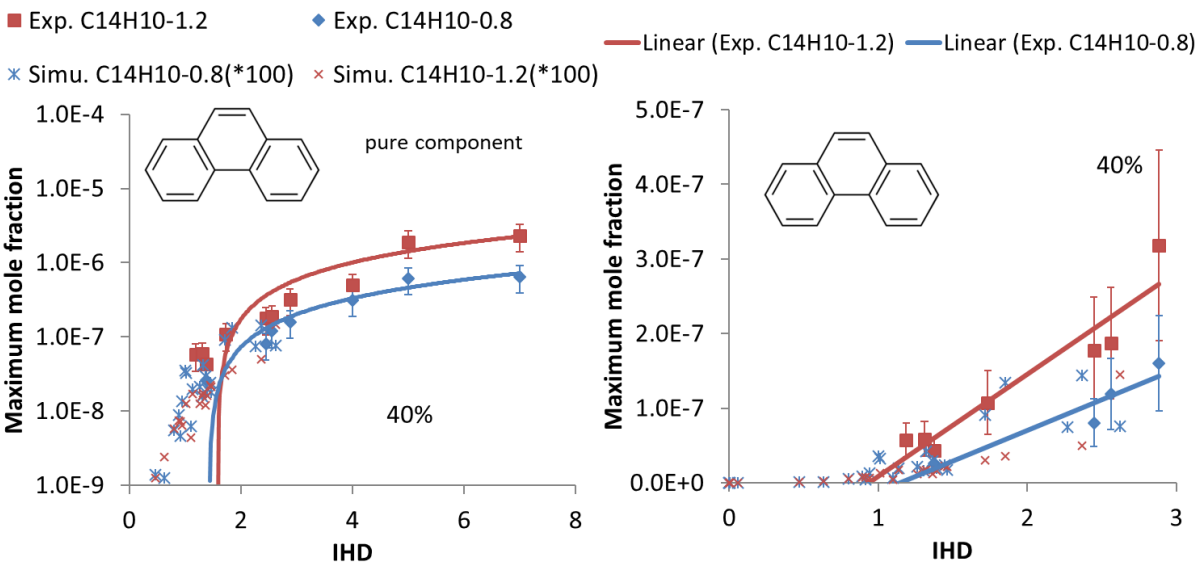

Fig. 26: Comparison of measured and predicted $C_{12}H_8$ (in model summation of ethynyl-naphthalene and acenaphthylene) and $C_{14}H_{10}$ (phenanthrene) maximum mole fraction of all fuels and neat components as a function of their IHD.

Overall, for soot modeling, the surrogate and the chemical kinetic model are highly sufficient. The small difference among gas species kinetics still provide room for improvement in the future. The above stated surrogate strategy and model validation presents few limitations to its interpretation. The GCxGC analysis provides information not detailed enough to resolve isomers which can have different reactivity. Here our assumption of use of multiple components, specifically cyclic components where the variation in the soot precursors is large, is helpful. Cyclic components of different molecular structure produce more diverse soot precursors predictions in contrast to one or two cyclic components used in the surrogate. This is visible in our comparison of various aromatics formed from different neat components presented in Part-II [19]. Here the aromatics formed from different cyclic component vary in the order of 2 or more which is beyond the uncertainty limit of the reaction mechanism or the surrogate definition. Definitely, our surrogate definition is not perfect, but given the restriction this is a reasonable approach and close to the description of a real fuel.

For the model related uncertainties, we computed the sensitivities to the change in *T* (along reactor length in the flow reactor) due to change in rate (preexponential factor A) at the temperatures where the deviations are high between model predictions and measurements. For this purpose, JS-A1 containing 14 fuel components is selected. For JS-A1, at both stoichiometries, this is found to be less than ±10% for O_2 and CO_2. The sensitivities to the change in maximum mole fractions of CO are ±4%, of CH_4 and C_2H_2 <±25%, C_2H_4 and C_3H_6 <±10% whereas the sensitivities of aromatics species C_6H_6, C_7H_8, and $C_{10}H_8$ are found to be <20%, <60%, and <45% respectively. Although this can consequently affect the model prediction, we believe the simulations of all 26 fuels with same mechanism allow to subordinate the uncertainty as the purpose of this study is the evaluation of how the fuel composition can be used to compare information of specific fuel intermediates and emissions formed.

The fuel-bound aromatics and in general cyclic molecules are mainly responsible for aromatic intermediate formation compare to n- and iso-paraffins. The main observation from the fuels and neat components can be listed as: (1) Different aromatics are responsible for soot precursors formation in individual hydrocarbons. It cannot be easily generalized. (2) Cyclo-paraffins, specifically bicyclic as well as cyclo-aromatics are equally important to consider for understanding of sooting behavior. (3) For fuels – mixtures of individual hydrocarbons - IHD which considers both cyclo-paraffins and aromatics, can be used to compare different fuels.

To summarize, the soot precursors formed in various conventional and alternative fuels are not investigated to the extent as analyzed in this work. In this context, the present study provides a valuable database on various soot precursors formed from large variety of fuels and importantly at comparable condition, useful in understanding the influence of fuel components and its assessment. A future study to infer difference in reactivity of fuels upon pressure variation can be of interest for practical applications. Additionally, the iso-paraffinic fuel will require more attention towards identification of exact molecular structure in order to model accurately. This will also require extension of reaction models.

7. Concluding Remarks

From the speciation data of individual hydrocarbons [19] and various fuels studied in this work, it is clear that the molecular fuel composition is an important aspect of a fuel for understanding its combustion and, more importantly, its emission behavior. Comparison of 26 fuels shows,

1. The major C_1-C_4 intermediate species formed during the combustion of the neat components in flow reactor, presents no specific or weak trends for few species with respect to global H/C ratio (Fig. 27, left). Although, trend specific to the fuels' n- and/or iso-paraffin or cyclic content can be drawn (Fig. 10 to Fig. 14). Compared to them, the fuels investigated showed linear relation to the H/C ratio for shown species (Fig. 27, right) and weak trend for C_3H_4 and C_4H_8 where the deviation is seen at lower H/C. The CH_4 and C_2H_4 are found to be independent to H/C ratio. In contrast, C_2H_6 and C_3H_6 shows slight increase and C_2H_2 and C_4H_6 shows slight decrease with H/C ratio, observation also in accordance with the measurements of 42 fuels in Part-I [28]. The formation of C_4H_4 shows strong decrease with increasing H/C ratio which is typically formed in the aromatics oxidation (low H/C).

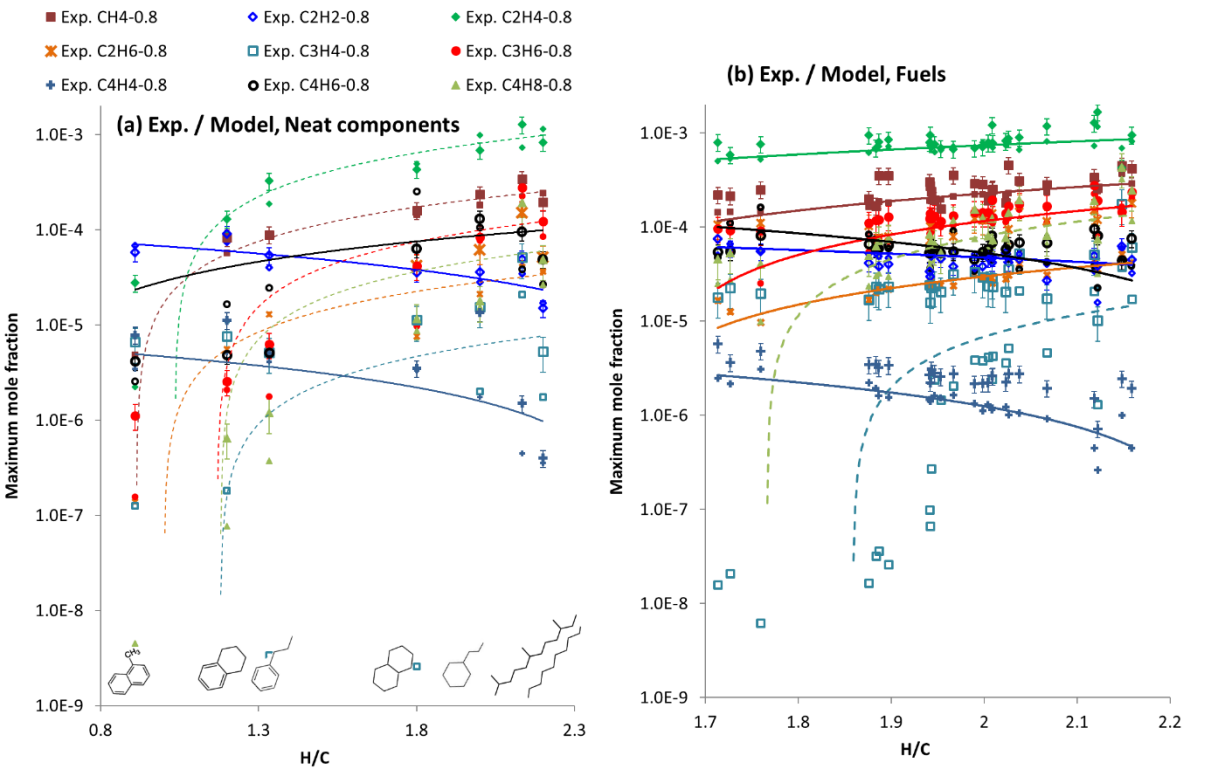

Fig. 27: Comparison of measured and modeled (smaller symbols compared to experiment) C_1-C_4 intermediates formed during the combustion of (a) maximum mole fractions of neat hydrocarbons and (b) fuels studied at flow reactor condition. Data points are at $\Phi = 0.8$, linear (note log scale) fitting lines are applied to modeled data.

2. 1- to 3-ring aromatics (Fig. 28) show linear increases for their maximum concentration with respect to the IHD, which also extends to larger aromatics in Fig. 29.

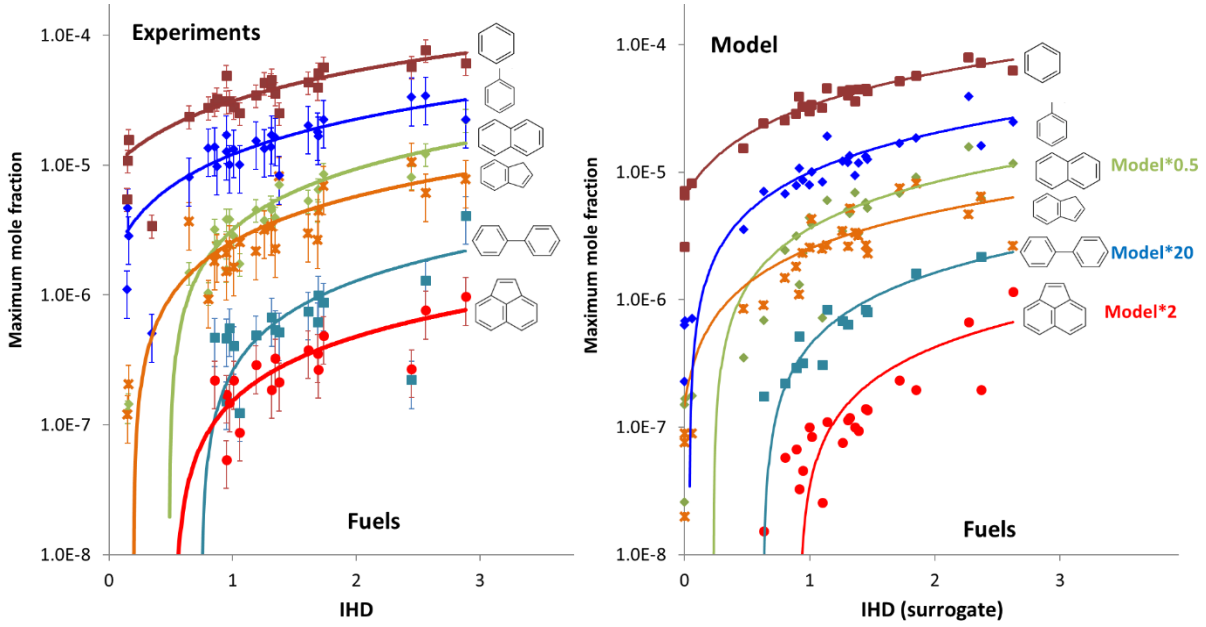

Fig. 28: Comparison of measured (left) and computed (right) maximum mole fractions of small aromatics measured in studied fuels as function of IHD. Data points are at Φ = 1.2, linear (note log scale) fitting lines are applied to it.

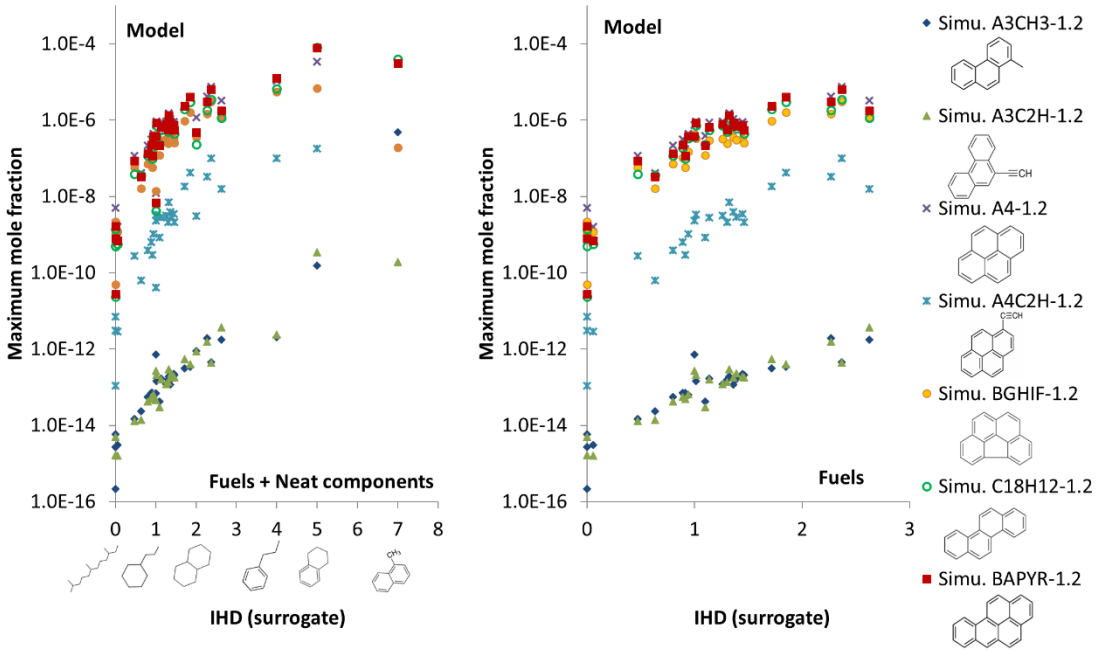

Fig. 29: Maximum mole fractions of larger aromatics as function of IHD obtained in numerical investigation of fuels and neat components (left) and in fuels (right). Only model results are available.

In general, the global reactivity of hydrocarbons is controlled by the bulk of linear-, branched-, and cyclic-paraffins present in a fuel however the sooting behavior is on the contrary controlled by the minor

amounts of cyclo-aromatics and aromatics present in a fuel. When studying fuels with the focus to soot emissions as shown in this work, irrespective of global kinetic tendency, the soot precursors formed will be very much dependent not only on the functional group of different molecular structure present but also on their amount and type.

In order to reproduce the complete initial chemical structural composition of a real fuel, it is important to know the molecular distribution using complex analysis methods [64] in agreement with the work of Dryer et al. [10]. As seen in an individual component, the soot precursor formed can vary depending on the molecular stability of the component. The major variations are seen among the mono- or di-aromatic molecules, bicyclic paraffins as well as cyclo-aromatics. Most of the fuels contain any of these components in a lesser extent compared to the bulk of n-, iso- and mono-cyclo-paraffins. Hence, one can evaluate the gross sooting behavior of a complex fuel by analyzing the amount of unsaturated and cyclic compounds present in the fuel, which is related to the IHD.

In conclusion, the here presented surrogate strategy and the associated chemical kinetic model, demonstrate an excellent performance on predicting global combustion characteristics as well as sooting tendencies of jet fuels. This single model is capable of resolving kinetic differences even within conventional and alternative jet fuels. The model is validated over a broad range of boundary conditions. The main soot precursor formation routes from cyclo-aromatics and aromatics as major jet fuel components are clearly identified and justified.

To conclude Part-III of our journey, this work's surrogate strategy and modeling approach are highly suitable for the future jet fuel development by jet fuel assessment as well as optimization. The model represents the foundation for the development of reduced chemical kinetic models for the application in CFD or novel engine development.

8. Acknowledgment

The authors gratefully acknowledge the DLR projects ECLIF and QSP Future Fuels, and the BMBF project Kopernikus P2X. Special thanks to all fuel contributors listed in Part-I for enabling such exhaustive study and Marc Mühlberg for his experimental contributions. Dr. M. Braun-Unkhoff is gratefully acknowledged for her fuel related activities.

This document contains supplemental material.

References:

[1] Jürgens S, Oßwald P, Selinsek M, Piermartini P, Schwab J, Pfeifer P, et al. Assessment of combustion properties of non-hydroprocessed Fischer-Tropsch fuels for aviation. Fuel Process Technol 2019;193:232-243.

[2] Kosir S, Stachler R, Heyne J, Hauck F. High-performance jet fuel optimization and uncertainty analysis. Fuel 2020;281:118718.

[3] Colket M, Edwards T, Williams S, Cernansky N, Miller DL, Egolfopoulos FN, et al. Development of an Experimental Database and Kinetic Models for Surrogate Jet Fuels. 45th AIAA Aerospace Sciences Meeting and Exhibit 2007; Paper No 2007-770.

[4] Schulz WD. Oxidation products of a surrogate JP-8 fuel. Prepr Am Chem Soc 1992;37:383–392.

[5] Dagaut P, Reuillon M, Cathonnet M. High Pressure Oxidation of Liquid Fuels from Low to High Temperature. 2. Mixtures of n-Heptane and iso-Octane. Combust Sci Technol 1994;103:315–336.

[6] Edwards T, Maurice LQ. Surrogate mixtures to represent complex aviation and rocket fuels. J Propul Power 2001;17:461–466.

[7] Ranzi E. A wide-range kinetic modeling study of oxidation and combustion of transportation fuels and surrogate mixtures. Energy Fuels 2006;20:1024-1032.

[8] Won S, Haas FM, Dooley S, Edwards T, Dryer FL. Reconstruction of chemical structure of real fuel by surrogate formulation based upon combustion property targets. Combust Flame 2017;183:39–49.

[9] Dooley S, Won SH, Heyne J, Farouk TI, Ju Y, Dryer FL, et al. The experimental evaluation of a methodology for surrogate fuel formulation to emulate gas phase combustion kinetic phenomena. Combust Flame 2012;159:1444−1466.

[10] Dryer FL, Jahangirian S, Dooley S, Won SH, Heyne J, Iyer VR, et al. Emulating the combustion behavior of real jet aviation fuels by surrogate mixtures of hydrocarbon fluid blends: Implications for science and engineering. Energy Fuels 2014;28:3474-3485.

[11] Narayanaswamy K, Pitsch H, Pepiot P. A component library framework for deriving kinetic mechanisms for multi-component fuel surrogates: Application for jet fuel surrogates. Combust Flame 2016;165:288–309.

[12] Kim D, Martz J, Abdul-Nour A, Yu X, Jansons M, Violi A. A six-component surrogate for emulating the physical and chemical characteristics of conventional and alternative jet fuels and their blends. Combust Flame 2017;179:86–94.

[13] Kerschgens B, Cai L, Pitsch H, Janssen A, Jakob M, Pischinger S. Surrogate fuels for the simulation of diesel engine combustion of novel biofuels. Int J Engine Res 2014;16:531-546.

[14] Cai L, Pitsch H. Optimized chemical mechanism for combustion of gasoline surrogate fuels. Combust Flame 2015;162:1623–1637.

[15] Honnet S, Seshadri K, Niemann U, Peters N. A surrogate fuel for kerosene. Proc Combust Inst 2009;32:485-492.

[16] Dooley S, Won SH, Chaos M, Heyne JS, Ju Y, Dryer FL, et al. A jet fuel surrogate formulated by real fuel properties, Combust Flame 2010;157:2333–2339.

[17] Westbrook C, Mehl M, Pitz WJ, Kukkadapu G, Wagnon SW, Zhang K. Multi-Fuel surrogate chemical kinetic mechanisms for real world applications. Phys Chem Chem Phys 2018;20:10588-10606.

[18] Luning Prak DJ, Jones MH, Trulove P, McDaniel AM, Dickerson T, Cowart JS. Physical and chemical analysis of Alcohol-to-Jet (ATJ) fuel and development of surrogate fuel mixtures. Energy Fuels 2015;29:3760−3769.

[19] Kathrotia T, Oßwald P, Naumann C, Richter S, Köhler M. Combustion kinetics of alternative jet fuels, Part-II: Reaction model for fuel surrogate, Accepted on 13.03.2021, Fuel (2021).

[20] Wang H, Dames E, Sirjean B, Sheen DA, Tango R, Violi A, et al. A high-temperature chemical kinetic model of n-alkane (up to n-dodecane), cyclohexane, and methyl-, ethyl-, npropyl and n-butyl-cyclohexane oxidation at high temperatures, JetSurF 2.0, Sept. 19, 2010 (http://melchior.usc.edu/JetSurF/JetSurF2.0).

[21] H. Pitsch group, Instituet für Technische Verbrennung, RWTH Aachen University, Germany.

[22] The CRECK Modeling Group, http://creckmodeling.chem.polimi.it/menu-kinetics.

[23] LLNL mechanism, https://combustion.llnl.gov/mechanisms.

[24] ASTM D7566-20b, Standard specification for aviation turbine fuel containing synthesized hydrocarbons. www.astm.org. Accessed 21 October 2020.

[25] Zschocke A, Scheuermann S, Ortner J. High biofuel blends in aviation (HBBA), 2012.

[26] DeWitt MJ, Corporan E, Graham J, Minus D. Effects of aromatic type and concentration in fischer-tropsch fuel on emissions production and material compatibility, Energy Fuels 2008;22:2411–2418.

[27] Graham JL, Striebich RC, Myers KJ, Minus DK, Harrison WE. Swelling of nitrile rubber by selected aromatics blended in a synthetic jet fuel, Energy Fuels 2006;20:759-765.

[28] Oßwald P, Zinsmeister J, Kathrotia T, Alves-Fortunato M, Burger V, van der Westhuizen R, Viljoen C, Lehto K, Sallinen R, Sandberg K, Aigner M, Le Clercq P, Köhler M, Combustion kinetics of alternative jet fuels, Part-I: Experimental flow reactor study. Accepted on 13.03.2021, Fuel (2021).

[29] Kathrotia T, Oßwald P, Köhler M, Slavinskaya N, Riedel U. Experimental and mechanistic investigation of benzene formation during atmospheric pressure flow reactor oxidation of n-hexane, n-nonane, and n-dodecane below 1200 K. Combust Flame 2018;194:426–438.

[30] Dagaut P, Karsenty F, Dayma G, Serinyel Z. Experimental and kinetic modeling of the oxidation of synthetic jet fuels and surrogates. Combust Sci Technol 2016;188:1705-1718.

[31] Won SH, Veloo PS, Dooley S, Santner J, Haas FM, Ju Y, Dryer FL. Predicting the global combustion behaviors of petroleum-derived and alternative jet fuels by simple fuel property measurements, Fuel 2016;168:34–46.

[32] Zhu Y, Li S, Davidson DF, Hanson RK. Ignition delay times of conventional and alternative fuels behind reflected shock waves, Proc Combust Inst 2015;35:241–248.

[33] G. Flora G, J. Balagurunathan J, S. Saxena S, J.P. Cain JP, Kahandawal SP, DeWitt MJ et al. Chemical ignition delay of candidate drop-in replacement jet fuels under fuel-lean conditions: A shock tube study. Fuel 2017;209:457–472.

[34] Valco DJ, Min K, Oldani A, Edwards T, Lee T. Low temperature autoignition of conventional jet fuels and surrogate jet fuels with targeted properties in a rapid compression machine. Proc Combust Inst 2017;36:3687-3694.

[35] Xu R, Wang K, Banerjee S, Shao J, Parise T, Zhu Y, et al. A physics-based approach to modeling real-fuel combustion chemistry - II. Reaction kinetic models of jet and rocket fuels. Combust Flame 2018;193:520-537.

[36] Wang H, Oehlschlaeger MA. Autoignition studies of conventional and Fischer–Tropsch jet fuels. Fuel 2012;98:249-258.

[37] Pelucchi M, Osswald P, Pejpichestakul W, Frassoldati A, Mehl M. On the combustion and sooting behavior of standard and hydro-treated jet fuels an experimental and modeling study on the compositional effects. Proc Combust Inst 2021;38 https://doi.org/10.1016/j.proci.2020.06.353.

[38] Saggese C, Singh AV, Xue X, Chu C, Kholghy MR, Zhang T, et al. The distillation curve and sooting propensity of a typical jet fuel. Fuel 2019;235:350–62.

[39] Kathrotia T, Riedel U. Predicting the soot emission tendency of real fuels - A relative assessment based on an empirical formula. Fuel 2020;261:116482.

[40] Oßwald P, Köhler M. An atmospheric pressure high-temperature laminar flow reactor for investigation of combustion and related gas phase reaction systems. Rev Sci Instrum. 2015;86:105–109.

[41] Osswald P, Whitside R, Schäffer J, Köhler M. An experimental flow reactor study of the combustion kinetics of terpenoid jet fuel compounds: farnesane, p-menthane and p-cymene. Fuel 2017;187:43-50.

[42] Kathrotia K, Naumann C, Oßwald P, Köhler M, Riedel U. Kinetics of ethylene glycol: the first validated reaction scheme and first measurements of ignition delay times and speciation data. Combust Flame 2017;179:172–184.

[43] Köhler M, Oßwald P, Xu H, Kathrotia T, Hasse C, Riedel U. Speciation data for fuel-rich methane oxy-combustion and reforming under prototypical partial oxidation conditions. Chem Eng Sci 2016;139:249–260.

[44] Huber ML, Lemmon EW, Diky V, Smith BL, Bruno TJ. Chemically authentic surrogate mixture model for the thermophysical properties of a coal-derived liquid fuel. Energy Fuels 2008;22:3249-3257.

[45] Pitz WJ, Mueller CJ. Recent progress in the development of diesel surrogate fuels. Prog Energy Combust Sci 2011;37:330–350.

[46] Battin-Leclerc F. Detailed chemical kinetic models for the low-temperature combustion of hydrocarbons with application to gasoline and diesel fuel surrogates. Prog Energy Combust Sci 2008;34:440–498.

[47] Mueller CJ, Cannella WJ, Bruno TJ, Bunting B, Dettman HD, Franz JA, et al. Methodology for formulating diesel surrogate fuels with accurate compositional, ignition-quality, and volatility characteristics. Energy Fuels 2012;26:3284−3303.

[48] Zhang HR, Eddings EG, Sarofim AF, Mayne CL, Yang Z, Pugmire RJ. Use of functional group analysis for the selection of surrogates for jet fuels. US Combustion Meeting, 2007.

[49] Puduppakkam KV, Liang L, Naik CV, Meeks E, Bunting BG. Combustion and emissions modeling of a gasoline HCCI engine using model fuels. Society of Automotive Engineers 2009, Paper No SAE 2009-01-0669.

[50] Colket M, Edwards T, Williams S, Cernansky NP, Miller DL, Egolfopoulos FN, et al. Identification of target validation data for development of surrogate jet fuels. AIAA Aerospace Sciences Meeting and Exhibit 2008 Paper no. AIAA-2008-0972.

[51] Olson DB, Pickens JC, Gill RJ. The effects of molecular structure on soot formation II. diffusion flames. Combust Flame 1985;62:43-60.

[52] Won SH, Haas FM, Tekawade A, Kosiba G, Oehlschlaeger MA, Dooley S, Dryer FL. Combustion characteristics of C4 iso-alkane oligomers: Experimental characterization of iso-dodecane as a jet fuel surrogate component, Combust Flame 2016;165:137–143.

[53] Davis SG, Law CK. Determination of and fuel structure effects on laminar flame speeds of C1 to C8 hydrocarbons, Comb Sci Tech 1998;140:427-449.

[54] Ji C, Dames E, Wang YL, Wang H, Egolfopoulos FN. Propagation and extinction of premixed C5–C12 n-alkane flames. Combust Flame 2010;157:277–287.

[55] Kelley AP, Smallbone AJ, Zhu D, Law CK. Laminar flame speeds of C5 to C8 n-alkanes at elevated pressures and temperatures. AIAA Aerospace Sciences Meeting. 2010, Paper No 2010-774.

[56] Richter S, Braun-Unkhoff M, Naumann C, Riedel U. Paths to alternative fuels for aviation. CEAS Aeronaut J 2018;9:389-403.

[57] DIPPR® Pro, Information and Data Evaluation Manager for the Design Institute for Physical Properties, Version 12.3.0 (2018).

[58] Riazi MR. Lee-Kesler method from characterization and properties of petroleum fractions. ASTM International 2005.

[59] Richter S, Naumann C, Kathrotia T, Braun-Unkhoff M, Riedel U. Synthesized alternative kerosenes – Characterization through experiments and modeling, Proc 9th European Combustion Meeting 2019; Paper No S5_All_20.

[60] Richter S, Braun-Unkhoff M, Kathrotia T, Naumann C, Kick T, Slavinskaya N, Riedel U. Methods and tools for the characterisation of a generic jet fuel. CEAS Aeronaut J 2019;10:925–935.

[61] Wang K, Xu R, Parise T, Shao J, Movaghar A, Lee DJ, et al. A physics-based approach to modeling real-fuel combustion chemistry – IV. HyChem modeling of combustion kinetics of a bio-derived jet fuel and its blends with a conventional Jet A. Combust Flame 2018;198:477-489.

[62] Corporan E, Edwards T, Stouffer S, Hendershott T, DeWitt M, Klingshirn C, et al. Impacts of Fuel Properties on Combustor Performance, Operability, and Emissions Characteristics, 55th AIAA Aerospace Sciences Meeting 2017; Paper No 2017-0380.

[63] Laskin A, Lifshitz A. Thermal decomposition of indene. Experimental results and kinetic modeling, Sym (Int) Combust 1998;27:313–320.

[64] Jürgens S, Riedinger M, Brühbach L, Navarrete Munoz A, Pfeifer P, Bauder U, et al. Potential of decentralized container-scale PtL plants for aviation: from crude to post-processed FT-SPK. Fuel Process Technol, In Preparation 2020.

Supplemental Material

to

Combustion Kinetics of Alternative Jet Fuels, Part-III: Fuel Modeling and Surrogate Strategy

Trupti Kathrotia*, Patrick Oßwald, Julia Zinsmeister, Torsten Methling, Markus Köhler

German Aerospace Center (DLR), Institute of Combustion Technology,

Pfaffenwaldring 38-40, 70569 Stuttgart, Germany

*Corresponding author: Trupti.Kathrotia@dlr.de

Table of Contents

1. PFR Inlet condition

Table 3: Summary of inlet conditions of measured aviation fuels and pure components used in the model

Fuels /Single components		Φ = 0.8 (1.2), 1 atm		
		Fuel mg/min	O_2 mg/min	Ar g/min
Fuels				
1	FT-Light	31.7	138.0 (92.0)	17.64
2	Farnesane	31.6	136.8 (91.2)	17.64
3	JS-B1	31.6	137.1 (91.4)	17.64
4	ATJ-SKA	31.7	138.2 (92.1)	17.64
5	JS-B3	31.5	135.7 (90.4)	17.64
6	Acc-HEFA50	31.4	135.0 (90.0)	17.64
7	E1_FSJF	31.3	133.4 (88.9)	17.64
8	E1_Ref1	31.1	132.1 (88.1)	17.64
9	E1_Ref2	31.1	132.1 (88.1)	17.64
10	E1_SSJF1	31.4	134.5 (89.7)	17.64
11	E1_SSJF2	31.4	134.8 (89.9)	17.64
12	E1_SSJF3	31.2	132.8 (88.5)	17.64
13	E2_Ref3	31.0	131.2 (87.5)	17.64
14	E2_Ref4	31.2	132.9 (88.6)	17.64
15	E2_SAJF1	31.3	133.9 (89.3)	17.64
16	E2_SAJF2	31.3	134.4 (89.6)	17.64
17	E2_SAJF3	31.2	132.6 (88.4)	17.64
18	JS_A1	31.2	132.6 (88.4)	17.64
19	JS_A1.3	31.3	134.0 (89.4)	17.64
20	JS_C1	30.7	127.9 (85.2)	17.64
21	S-IPK-A	31.3	133.8 (89.2)	17.64
22	S-HN1	31.5	135.6 (90.4)	17.64
23	S-HN2	30.7	127.4 (84.9)	17.64
24	S-LD2	30.8	128.74 (85.8)	17.64
25	S-IPK	31.7	137.65 (91.8)	17.64
26	S-LD1	31.1	132.9 (88.6)	17.64
Single components				
1	n-Decane	31.7	138.3	17.64
2	Farnesane	31.6	136.8 (91.2)	17.64
3	n-Propylcyclohexane (PCH)	31.3	133.8 (89.2)	17.64
4	n-Propylbenzene (PBZ)	29.8	119 (79.3)	17.64
5	Decalin	30.8	129.4 (86.3)	17.64
6	Tetralin	29.5	116 (77.3)	17.64
7	Methylnaphthalene (MN)	28.8	109.5 (73)	17.64

2. Distillation curves

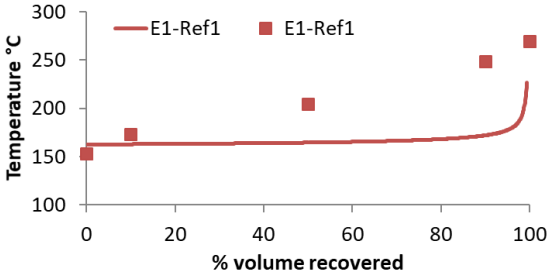

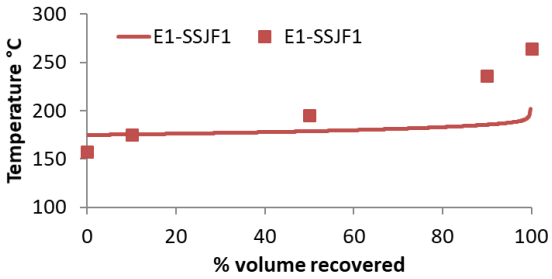

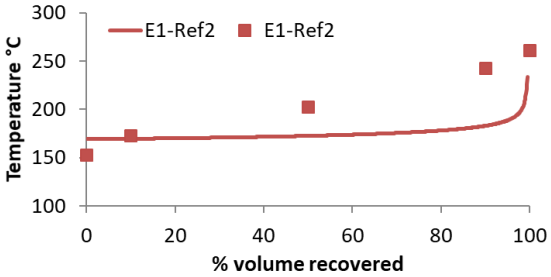

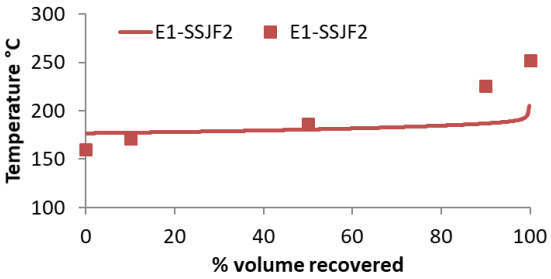

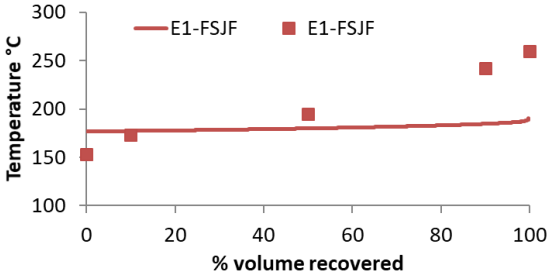

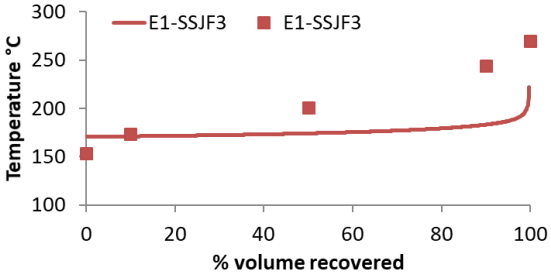

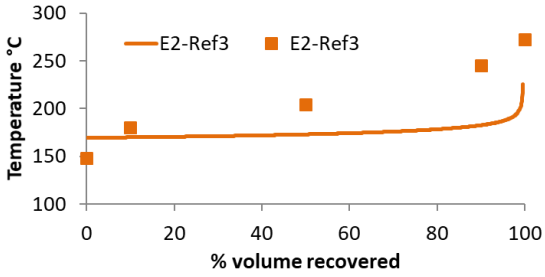

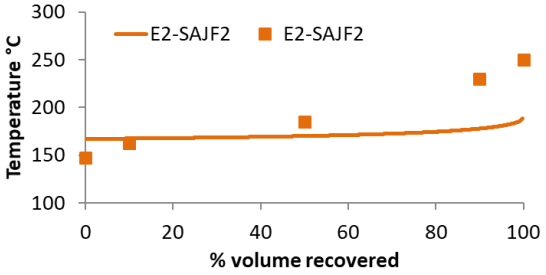

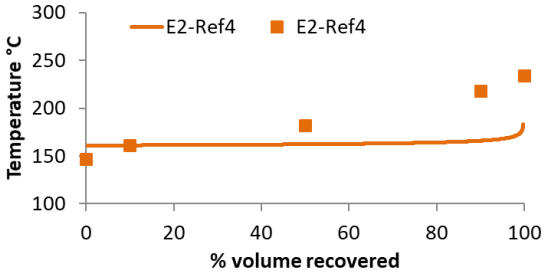

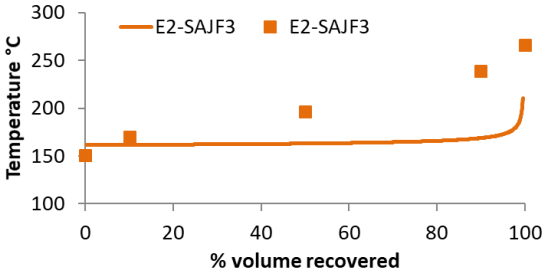

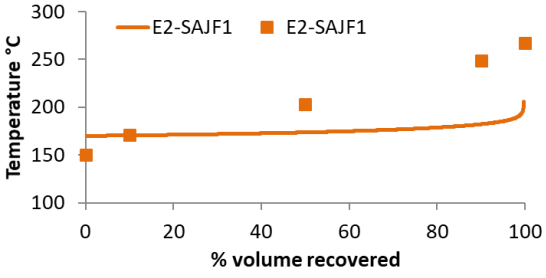

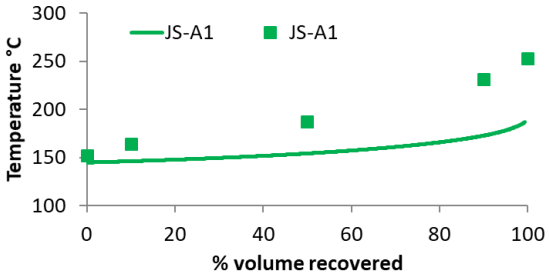
JS-A1
JS-A1
Temperature °C
% volume recovered

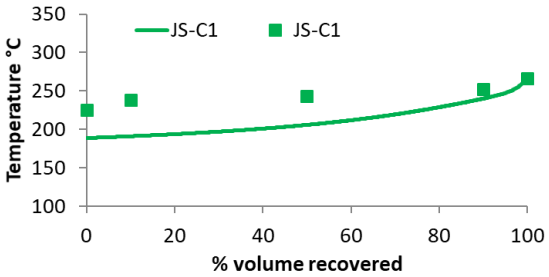
JS-C1
JS-C1
Temperature °C
% volume recovered

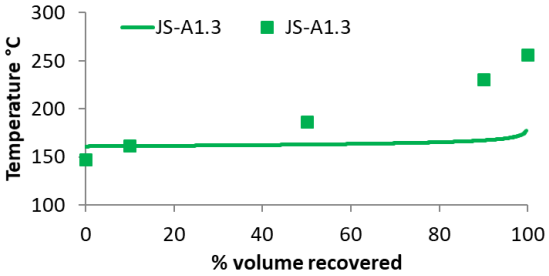
JS-A1.3
JS-A1.3
Temperature °C
% volume recovered

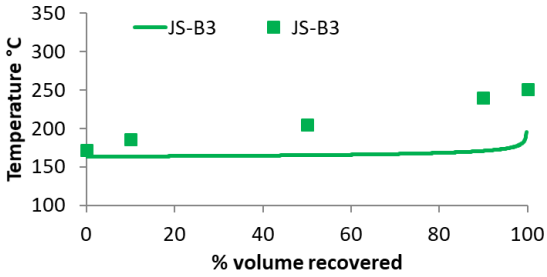
JS-B3
JS-B3
Temperature °C
% volume recovered

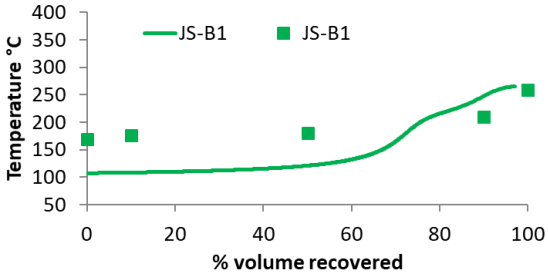
JS-B1
JS-B1
Temperature °C
% volume recovered

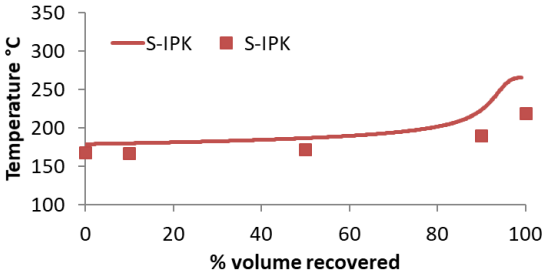
S-IPK
S-IPK
Temperature °C
% volume recovered

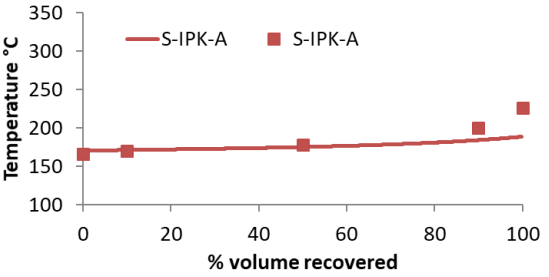
S-IPK-A
S-IPK-A
Temperature °C
% volume recovered

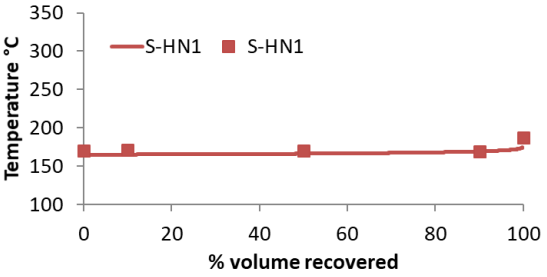
S-HN1
S-HN1
Temperature °C
% volume recovered

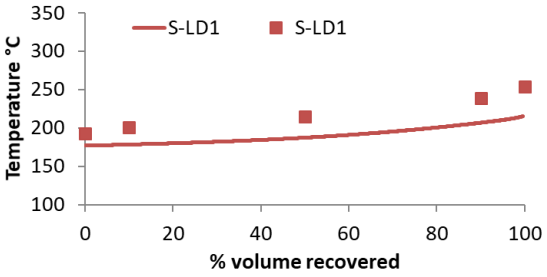
S-LD1
S-LD1
Temperature °C
% volume recovered

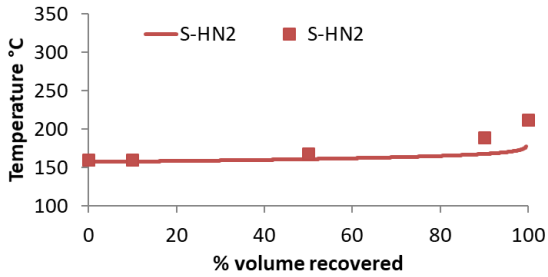
S-HN2
S-HN2
Temperature °C
% volume recovered

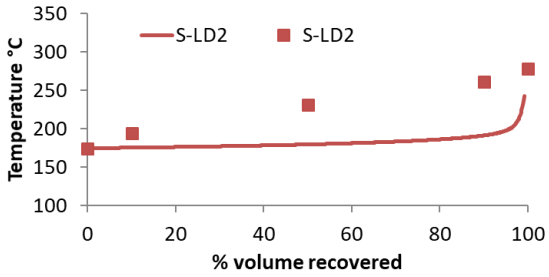
S-LD2
S-LD2
Temperature °C
% volume recovered

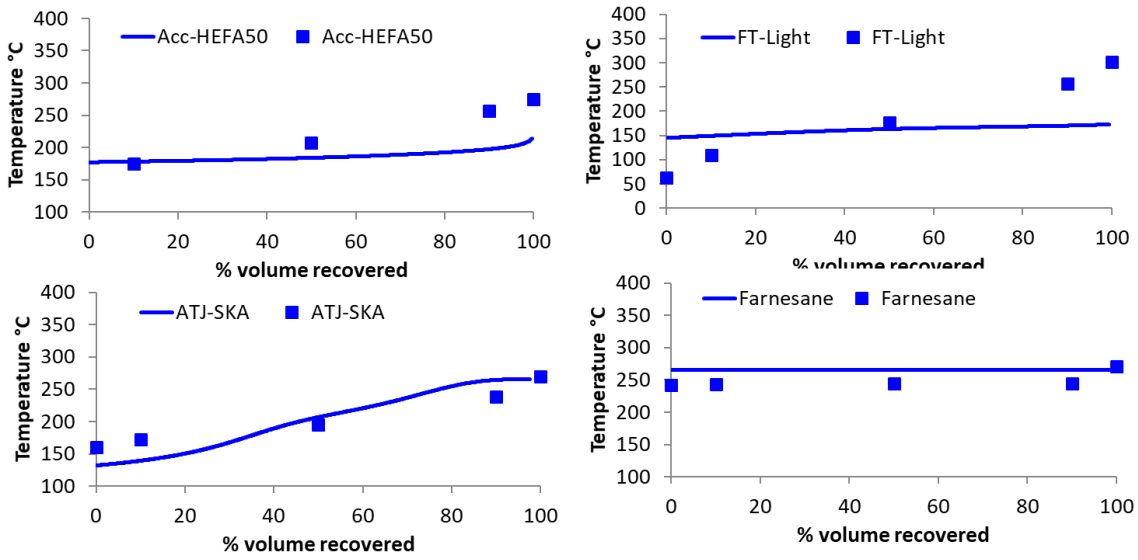

Fig. 1: Comparison of measured (symbols) and predicted (curve) distillation curves of all fuels and fuel surrogates studied in this work.

3. Major formation routes of C1-C4 hydrocarbons

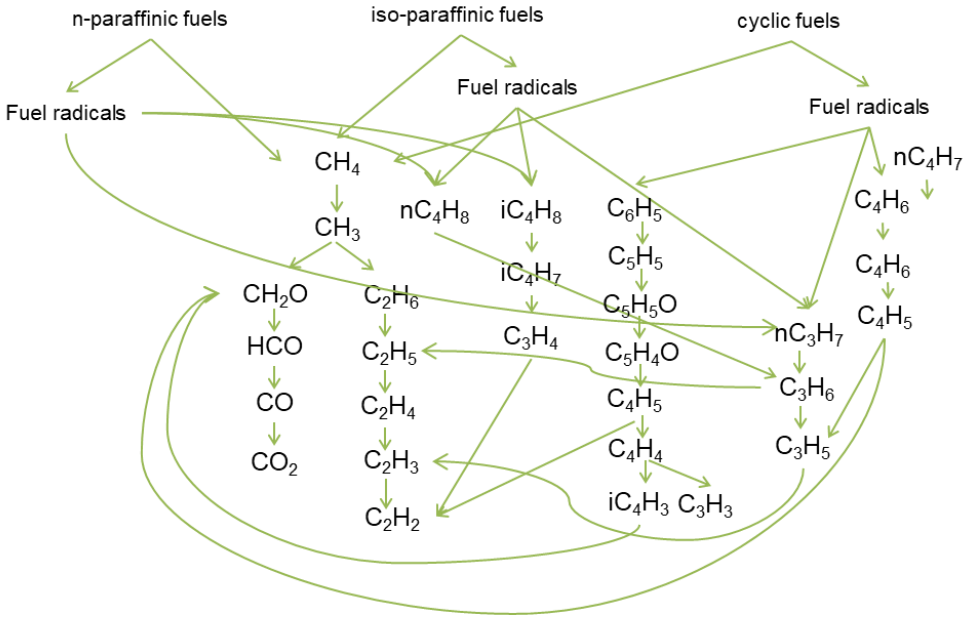

Fig. 2: Major formation routes of C1-C4 hydrocarbons from fuel components.

4. Decomposition routes of hydrocarbons

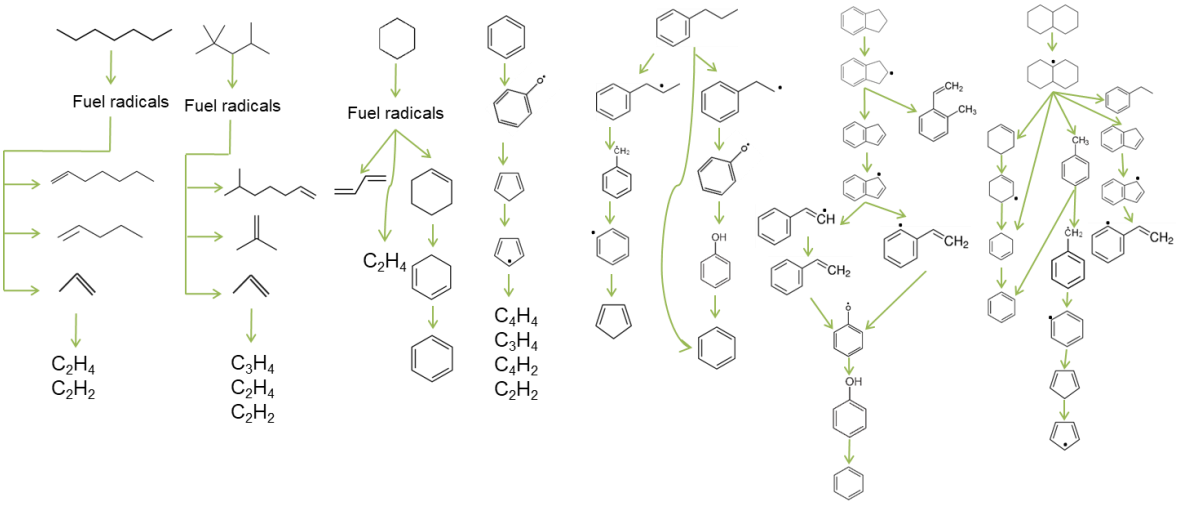

Fig. 3: General decomposition routes of various hydrocarbons [Kathrotia2021].

[Kathrotia2021] Kathrotia T, Oßwald P, Naumann C, Richter S, Köhler M. Combustion kinetics of alternative jet fuels, Part-II: Reaction model for fuel surrogate, Manuscript submitted to Fuel (2020).